NNANO-18091898B
Second revision

NEURONAL FIRING MODULATION BY A MEMBRANE-TARGETED PHOTOSWITCH

Mattia Lorenzo DiFrancesco[1,2§], Francesco Lodola[3§], Elisabetta Colombo[1,2§], Luca Maragliano[1,2], Mattia Bramini[1,2†], Giuseppe Maria Paternò[3], Pietro Baldelli[2,4], Mauro Dalla Serra[5,6], Lorenzo Lunelli[6,5], Marta Marchioretto[5,6], Giorgio Grasselli[1,2], Simone Cimò[3,7], Letizia Colella[7], Daniele Fazzi[8], Fausto Ortica[9], Vito Vurro[3], Cyril Giles Eleftheriou[1,2†], Dmytro Shmal[1,2], José Fernando Maya-Vetencourt[1,2†], Chiara Bertarelli[3,7§], Guglielmo Lanzani[3§*], Fabio Benfenati[1,2§*]

[1]Center for Synaptic Neuroscience, Istituto Italiano di Tecnologia, Largo Rosanna Benzi 10, 16132 Genova, Italy; [2]IRCCS Ospedale Policlinico San Martino, Genova, Italy; [3]Center for Nano Science and Technology, Istituto Italiano di Tecnologia, Via Pascoli 10, 20133, Milano, Italy; [4]Department of Experimental Medicine, University of Genova, Viale Benedetto XV, 3, 16132 Genova, Italy; [5]Istituto di Biofisica, Consiglio Nazionale delle Ricerche, via alla Cascata 56/C, 38123 Trento, Italy; [6]Laboratory of Biomarker Studies and Structure Analysis for Health, Fondazione Bruno Kessler, Via Sommarive 18, 38123 Trento, Italy; [7]Dipartimento di Chimica, Materiali e Ingegneria Chimica "*Giulio Natta*", Politecnico di Milano, Piazza L. da Vinci 32, 20133 Milano, Italy; [8]Department of Chemistry, Institut für Physikalische Chemie, University of Cologne, Luxemburger Str. 116, D -50939 Köln, Germany; [9] Department of Chemistry, Biology and Biotechnology, Università degli Studi di Perugia, via Elce di Sotto 8, 06123 Perugia, Italy.

[§]equal contribution

[†]present address: Mattia Bramini, Department of Applied Physics, Faculty of Sciences, University of Granada, C/Fuentenueva s/n, 18071-Granada, Spain; Cyril Giles Eleftheriou, Departments of Ophtalmology and Neurology, Burke Medical Research Institute, Weil Medical College of Cornell University, White Plains, NY, USA; José Fernando Maya-Vetencourt, Department of Biology, University of Pisa, Pisa, Italy.

Short title: Membrane-targeted photochromic probes for neuronal excitation

Keywords: photoexcitation, azobenzene derivatives, capacitance, lipid rafts

***Corresponding authors:**

Guglielmo Lanzani, PhD, Center for Nano Science and Technology, email: guglielmo.lanzani@iit.it

Fabio Benfenati, MD, Center for Synaptic Neuroscience and Technology, email: fabio.benfenati@iit.it

ABSTRACT

Optical technologies allowing modulation of neuronal activity at high spatio-temporal resolution are becoming paramount in neuroscience. In this respect, azobenzene-based photoswitches are promising nanoscale tools for neuronal photostimulation. Here we engineered a novel light-sensitive azobenzene compound (Ziapin2) that stably partitions into the plasma membrane, and causes its thinning through trans-dimerization in the dark, resulting in an increased membrane capacitance at steady state. We demonstrated that in neurons loaded with the compound, millisecond pulses of visible light induce a transient hyperpolarization followed by a delayed depolarization that triggers action potential firing. These effects are persistent and can be evoked *in vivo* up to 7 days, proving the potential of Ziapin2 for the modulation of membrane capacitance in the millisecond time scale, without directly affecting ion channels or local temperature.

Optical technologies for the modulation of neuronal activity are becoming increasingly important in cell biology and neuroscience (1,2). Indeed, the possibility to obtain neuronal excitation or inhibition on demand not only has allowed an unprecedented power in interrogating and dissecting out the function of specific brain circuits, but has also opened new perspectives for treating neurological and psychiatric diseases (3).

Optogenetics is the pioneering technique in neuro-optical technologies (3,4). Similar to optogenetics, the generation of tethered azobenzene photoswitches targeted to membrane bilayers (5-10) or linked to ion channels (11-16) allowed modulating ion channel dynamics and/or the electrical properties of the membrane in a light-dependent fashion.

Extracellular photostimulation by light-sensitive interfaces represent an alternative strategy. Extended planar organic interfaces were used to achieve light-dependent modulation of the electrical state of neurons (17-21) that, at high light intensities, also involved a thermal effect (19,22,23). Similar results were obtained by increasing the local temperature with IR illumination of absorbers in contact with cells (24,25), thus increasing the membrane capacitance and in turn depolarizing the target cell. However, temperature rises of several degrees can be harmful to neurons, particularly if administered repeatedly.

In this work, we engineered an amphiphilic azobenzene-based photoswitch to obtain an intramembrane actuator for inducing *heatless* membrane stress/perturbation upon irradiation with visible light. Our photochromic actuator, named Ziapin2, contains two ionic terminated alkyl chains that align with the phospholipid headgroups, and the azobenzene moiety end-capped with a hydrophobic azepane that can be folded/unfolded in a light-dependent manner. Incubation of the compounds with primary neurons showed that the molecules spontaneously partition into the membrane, where they preferentially distribute to membrane rafts and induce membrane thinning and increased capacitance through trans-dimerization. *Trans*→*cis* isomerization triggered by millisecond pulses of visible light displaces the hydrophobic end-group from the membrane core and causes a sharp and transient decrease in capacitance due to membrane relaxation that generates a transient hyperpolarization. In

74 neurons, the fast return of capacitance to the steady-state level is followed by action potential firing.
75 Persistent light-evoked stimulation of Ziapin2-labeled mouse somatosensory cortex activity is also
76 observed *in vivo*.
77
78

Synthesis and characterization of Ziapin2

Amphiphilic azobenzenes have been previously reported for different applications (5). Herein, we were inspired by the initial work of Fujiwara and Yonezawa who showed that an aliphatic amphiphilic azobenzene derivative was able to change the capacitance of black lipid membranes in response to prolonged UV illumination (6-8), and by the subsequent work of Bazan and collaborators who reported that non-photochromic water-soluble distyrylstilbene oligoelectrolytes (DSSN+), capped at each end with nitrogen-bound terminally charged pendant groups, effectively localized to the membrane modifying its optical and electronic properties (9,10). Here, we combined a hydrophobic backbone containing the photoactive 4-4' diaminoazobenzene substituted on one side with an azepane and on the opposite side with alkyl chains that are ω-substituted with cationic groups, i.e. pyridinium salts. The combination of the alkyl-substituted azobenzenes with a capping cation leads to amphiphilic species able to dwell inside the cell membrane (Ziapin2; **Fig. S1** and Online Methods).

Azobenzene molecules undergo *trans*→*cis* isomerization upon illumination with visible radiation (**Fig. 1a**), with the reverse *cis*→*trans* isomerization driven by either light or thermal excitation (26-28). Ziapin2 shows the typical UV-Vis absorption features of para amino-substituted azobenzenes, with a strong absorption peak centered at 470 nm (**Fig. 1b**), attributed to the $\pi \rightarrow \pi^*$ transitions of the *trans* isomer (28). Irradiation with blue light leads to *trans*→*cis* isomerization as seen from the concomitant bleaching of the *trans* isomer absorption and increase of the *cis* conformer absorption. A well-defined and relatively fast collective photoswitching dynamics of Ziapin2 in DMSO was detected by measuring the decrease of absorbance at 470 nm *vs* irradiation time (**Fig. 1c**). Also the steep time-dependent decrease in Ziapin2 photoluminescence (PL) at 540 nm in DMSO upon blue light exposure (**Fig. 1d,e)** can be related to the photoisomerization-induced reduction in the *trans* population, due to the negligible PL quantum yield of the *cis* isomer. Indeed, the excitation profile of the normalized change in PL (**Fig. S2a,b**) follows the absorption profile of the *trans* isomer, confirming its relation to the isomerization process. We estimated a *trans*→*cis* photoisomerization coefficient $k\tau = 16.9$ cm^2 J^{-1} and a *cis*→*trans* thermal rate $y = 0.06$ s^{-1} (red line in **Fig. 1e**; see Online Methods). A complete

suppression of the Ziapin2 photoswitching was observed in water as compared to DMSO (**Fig. 1f**), likely caused by strong aggregation of Ziapin2 (29). The formation of aggregates was also corroborated by the redshift of Ziapin2 PL (82 nm, **Fig. S2c,d**) and absorption (22 nm, **Fig. S2e**) in water. To disentangle a possible fast relaxation behavior from a complete isomerization suppression of Ziapin2 in water, we carried out time-resolved PL measurements in the picosecond time regime (**Fig. S2f**). These data indicate a strong difference in the deactivation path for Ziapin2 in the two solvents, with a relatively fast emission lifetime in DMSO (8 ps), consistent with the photoisomerisation reaction, and a marked slowdown of the lifetime in water (26 ps) due to the formation of molecular aggregates. Interestingly, in SDS we observed a 25% decrease of the lifetime when compared to water, an effect that can be attributed to the partially recovered isomerization ability of membrane-embedded Ziapin2. Aggregation was also investigated by UV-Vis and PL spectra as a function of concentration (**Fig. S3a-c)** and upon water addition (**Fig. S3d-f)**. While normalized absorption spectra of Ziapin2 show little dependence on concentration, PL exhibits a linear redshift, suggesting the occurrence of an excited state interaction. Abs/PL spectra for Ziapin2 at fixed concentration (25 μM) and different DMSO/water ratios show a growing a redshift upon water addition alongside an increase of PL intensity **(Figure S3d-f)**. The broad, featureless and Stokes-shifted emission suggests the formation of aggregates with an excimeric-like deactivation, similarly to what observed for confined azobenzene derivatives in nanostructured silica (30).

Interestingly, the PL spectra of Ziapin2 in sodium dodecyl sulfate (SDS) micelles, mimicking the bilayer environment (31), and in cell membranes essentially coincide lying between DMSO and water spectra (**Fig. S2c**). Total internal reflection fluorescence (TIRF) microscopy on model bilayers composed of either phosphatidylcholine (PC) or a mixture of PC, cholesterol and sphingomyelin (SM), mimicking the composition of lipid rafts, confirmed the spectral overlap between Ziapin2 PL in SDS micelles, model membranes and raft-like membranes (**Fig. S4**). Similarly, the photoswitching dynamics in either SDS micelles (**Fig. S2d**) or cell membranes (**Fig. 1f**) resulted intermediate between the fast photoswitching behavior in DMSO and the frozen photodynamics observed in aqueous media.

The non-exponential PL decay in the cell membrane **(Fig. 1g**) reflects the relaxation time distribution in disordered environments, such as lipid rafts or local phase/thickness changes. Although the molecular event of photoisomerization occurs in the sub-ps time scale, the sizable change observed in the time evolution of the isomeric populations in the ensemble is associated with a macroscopic fraction of isomerized molecules. All these findings suggest that the partition of the molecule in lipid membranes avoids the aggregation of Ziapin2, enabling effective isomerization and light-controlled photoswitching.

Ziapin2 increases membrane capacitance

We performed Molecular Dynamics (MD) simulations placing one molecule of Ziapin2 in *trans* conformation in the water region, parallel to a PC membrane and in different orientations. In three simulations, the molecule entered the bilayer within 100 ns, and remained in the membrane for the rest of the trajectory (**Fig. 2a,b**). In all cases Ziapin2 entered the membrane by first piercing it with the azobenzene side, and then moving towards the center of the bilayer by keeping the elongated axis almost parallel to the bilayer normal (**Fig. 2a**; I-IV). The insertion stopped when the positively charged pyridine rings were at the level of the lipid heads, coordinated by phosphate groups. Interestingly, in a different simulation, one Ziapin2 molecule placed at the center of the bilayer and parallel to it, reached very rapidly (< 5 ns) the same equilibrium position. The insertion process was quantitatively studied by calculating the associated free energy profile (**Fig. 2c**). We found essentially no barrier for Ziapin2 adsorption in the membrane, a pronounced minimum at the equilibrium position spontaneously obtained before, and a barrier for membrane desorption to water of ≅12 kcal·mol^{-1} (0.52 eV).
Before studying the cellular distribution and effects of Ziapin2 in neurons, we demonstrated that Ziapin2 did not elicit any toxic or inflammatory reaction in neurons (**Fig. S5, Fig. S6**).
Next, primary hippocampal neurons loaded with Ziapin2 were live-stained with the plasma membrane reporter Cell Mask and subjected to 3D confocal imaging (**Fig. 2d**). The quantification revealed that more than 70% of Ziapin2 was localized to the neuronal surface, with a coverage of ≈15% of the total

membrane surface (**Fig. 2d-f**), that progressively decreased over time ($t_{1/2}$ = 36.4 h, **Fig. S7a**). The occurrence of fluorescence resonance energy transfer (FRET) between Ziapin2 and Cell Mask further demonstrates that Ziapin2 is strictly localized to the membrane bilayer (**Fig. S7b,c**).

Given the punctate distribution of Ziapin2 fluorescence on the plasma membrane, we evaluated the colocalization of Ziapin2 with lipid rafts (32) by live labeling with cholera toxin β-subunit, and high-resolution fluorescence microscopy with structured light (SIM; **Fig. 2e**). Interestingly, the percentage of Ziapin2 colocalizing with lipid rafts (≈60%) was only slightly smaller than that observed with Cell Mask and covered a significantly higher proportion (≈25%) of the total raft surface with respect to Cell Mask (**Fig. 2e,f**). To unambiguously demonstrate the propensity of Ziapin2 for lipid rafts, we treated primary neurons with methyl-β-cyclodextrin (MβCD) to partially deplete membrane cholesterol and decrease the density of lipid rafts (≈50% decrease based on Filipin staining; **Fig. S8a; Fig. 2g**). Strikingly, MβCD markedly altered the punctate distribution of Ziapin2 in the membrane, by decreasing the density of Ziapin2-positive puncta and increasing the Ziapin2-positive areas, indicative of release of the probe from the rafts and its dispersion within the membrane (**Fig. 2g,h**).

Spatially resolved membrane thickness maps calculated from simulations of multiple Ziapin2 molecules in *trans* or *cis* conformations revealed the presence of thinner bilayer regions in the *trans* case (**Fig. 3a; Fig. S9**). Indeed, *trans* Ziapin2 molecules anchored to the opposite leaflets of the membrane form dimers via backbone interaction, pulling lipid heads towards the center of the bilayer and resulting in a local depression of the membrane (**Fig. 3a**, left panels). Conversely, when Ziapin2 is in *cis* conformation, the hydrophobic tails of opposed molecules are too far from each other to dimerize, leaving the membrane thickness unperturbed (**Fig. 3a**, right panels). A similar bilayer depression, associated with *trans* Ziapin2 dimerization, was observed in a lipid raft model (**Fig. 3b**).

We then investigated by atomic force microscopy (AFM) whether insertion of Ziapin2 in artificial membranes affects bilayer thickness. According to MD predictions, incorporation of *trans* Ziapin2 in unilamellar liposomes composed of either PC or a raft-like mixture induced a significant reduction in

membrane thickness that was more extended and pronounced in the raft-mimicking environment (**Fig. 3c,d; Fig. S10**).

Given the inverse proportionality between capacitance and thickness, we measured the capacitance of stably preformed planar membranes of PC or raft-like composition after addition of *trans* Ziapin2 to one or both sides of the bilayer. Unilateral addition of Ziapin2 increased the bilayer capacitance in both types of membrane, an effect that became significantly larger when Ziapin2 was added on both sides (**Fig. 3e; Fig. S11a**).

We then checked whether Ziapin2 in the dark had any effect on capacitance in a simple cell model (Hek293; **Fig. 3f**). The addition of Ziapin2 induced a significant increase in capacitance (32.1 ± 1.7 pF), likely attributable to the bilayer thinning caused by Ziapin2 *trans*-dimerization, while the DMSO vehicle was ineffective (26.4 ± 1.4 pF; see **Suppl. Materials** and **Fig. S11b-d**).

Light-induced neuronal activity by Ziapin2 *in vitro*

MD simulations predict that light-induced *trans*→*cis* photoconversion of Ziapin2 would relax the membrane towards its native thickness **(Fig. S12**), thereby reversing the effect on membrane capacitance. When light stimuli were administered to Ziapin2-loaded Hek293 cells, the increased capacitance returned toward basal levels (mean decrease ± sem: 4.4 ± 0.5 pF), while vehicle-loaded cells did not respond to light (**Fig. S13a**; cfr Fig. 3f). Such effect was associated with membrane hyperpolarization, peaking ≈13 ms after light onset and followed by a delayed depolarization (**Fig. S13b,c**), as reproduced by a numerical simulation of the membrane equivalent circuit (**Fig. S13d**).

We next tested the physiological effects of Ziapin2 in primary hippocampal neurons (**Fig. 4a**). In the dark, a significant capacitance increase was observed (from 32.4 ± 1.7 pF to 53.3 ± 6.0 pF; **Fig. 4b**), without significant changes in other passive membrane properties (**Figs. S11e-g** and **S14a**). When Ziapin2-loaded neurons were photostimulated, a fast and significant capacitance drop (mean decrease ± sem: 6.5 ± 1.1 pF) was observed, followed by a slow return to the pre-illumination level (**Fig. 4b**). The change in capacitance peaked few ms after light onset and was not significantly

different between 20 and 200 ms of light stimulation. Notably, a significant correlation was observed between the *trans* Ziapin2 capacitance increase and the light-induced capacitance drop (**Fig. 4b**). Ziapin2-labeled neurons showed a biphasic modulation of the membrane potential characterized by an early hyperpolarization, with a time course overlapping with the capacitance change, followed by a delayed depolarization of similar amplitude (**Fig. 4c,d**). While the hyperpolarization peak occurred with similar latency with 20 or 200 ms, the peak depolarization was delayed with 200 ms stimuli (**Fig. 4e**). To distinguish intrinsic effects from the effects of the reverberant network of synaptic connections, we employed blockers of excitatory and inhibitory synaptic transmission. Under these conditions, the magnitude and timing of hyperpolarization were unaffected (**Fig. 4c,d**; p=0.79 and p=0.69, Mann-Whitney *U*-test), while the amplitude of the depolarization was significantly decreased (**Fig. 4c,d**; p<0.01 for both 20 and 200 ms stimuli, Mann-Whitney *U*-test), similarly to that observed in Hek293 cells (**Fig. S13b,c**). These data indicate that light-induced hyperpolarization is an intrinsic effect resulting from the drop in capacitance, while the late depolarization response of neurons is amplified by the network synaptic transmission.

We then ran voltage-clamp experiments in Ziapin2-loaded neurons to build I/V plots of the light-induced transient capacitive current. Light stimulation (20 ms) elicited outward and inward currents at negative and positive potentials respectively, with an inversion at approximately 0 mV, as expected by a pure capacitive current. Consistently, no changes were observed in the I/V plots when choline replaced extracellular Na^+, or a cocktail of ion channel blockers for passive and active conductances was used (**Fig. S15a,b**; see Online Methods). These treatments also left unaltered the hyperpolarization response to light when the recording was switched to current-clamp (**Fig. S15c,d**). The hyperpolarization response to light of neurons that had been partially depleted of membrane cholesterol by MβCD (see above; **Fig. S8a,b**) was then investigated. Cholesterol depletion reduced the amplitude of light-evoked hyperpolarization in Ziapin2-labeled neurons, suggesting that clustering of Ziapin2 molecules at cholesterol-enriched membrane domains is essential for enhancing the light-dependent effects on membrane thickness (**Fig. S8b,c**).

Morphological studies indicated that ~30% of the initial Ziapin2 labeling was present on the plasma membrane 7 days after loading, with a parallel reduction of light-evoked hyperpolarization with respect to acute Ziapin2 (**Fig. 4f, Fig. S7**). However, the delayed depolarization was only slightly decreased (**Fig. 4f**), suggesting that the reduced membrane Ziapin2 concentration decreases the extent of light-evoked capacitance drop, leaving the return to basal capacitance relatively unaffected.

The steady increase in membrane capacitance induced by Ziapin2 in the dark significantly increased the rheobase and slowed down APs spontaneous frequency. Analysis of the AP waveform by phase plane plot revealed a slowdown of the rising and repolarizing slopes and an increased AP half-width, in the absence of changes in AP amplitude (**Fig. S14b,c**). We then examined the ability of light stimulation to elicit APs in Ziapin2-loaded neurons acutely and 7 days after membrane labeling (**Fig. 5a-c**). Light stimulation elicited a significant increase of AP frequency (**Fig. 5a**). Such result was even more striking in the presence of synaptic blockers that abolished spontaneous light-independent firing (**Fig. 5b**). Light-evoked firing was persistent over time, as shown 7 days after Ziapin2 labeling in the presence of synaptic blockers (**Fig. 5c**). Peristimulus time histogram (PSTH) analysis showed that light reliably induced AP firing activity. AP firing peaked after light offset for short stimuli and during the light phase for long stimuli (**Fig. 5d-g**). Interestingly, repetitive firing was obtained with light pulse trains of 200 ms at 1 Hz or 20 ms at 5 Hz, with only occasional failures (**Fig. 5h**). Phase plane plot analysis of AP waveforms (**Fig. 5i**) revealed that light-evoked APs were characterized by increased rising/repolarization slopes and peak amplitudes, consistent with the light-induced drop in membrane capacitance.

Comparable light-evoked physiological effects of Ziapin2 described in murine neurons were also observed in human neurons differentiated from induced pluripotent stem cell (iPSC) clones generated from skin fibroblasts of healthy volunteers (**Fig. S16;** 33). We also compared the Ziapin2 effects with the photostimulation of primary neurons transduced with the ultrafast microbial opsin ChETA, a light-dependent cationic channel (34) (**Fig. S17**). As expected from a light-gated ion channel, ChETA induced a larger V_m modulation than Ziapin2 at all stimulus durations, although the peak-to-peak

difference reached significance only in the presence of synaptic blockers (**Fig. S17a**). Notably, no significant differences were observed in the latency to the peak V_m change in the absence of APs (**Fig. S17a**), as well as in the light-induced firing probability measured both at the resting membrane potential (-53.6 ± 0.9 mV) and with neurons depolarized near threshold (-35 mV; **Fig. S17c**). However, ChETA was faster in the latency to the first light-induced AP (**Fig. S17d**). Waveform analysis of light-evoked APs failed to detect differences between ChETA- and Ziapin2-labeled neurons, indicating that the light-induced decrease in capacitance in Ziapin2-loaded neurons normalized the AP dynamics (**Fig. S17e**).

Light-induced cortical activity by Ziapin2 *in vivo*

Ziapin2 or vehicle was injected in the somatosensory cortex of mice, subsequently implanted with a multielectrode array coupled with an optical fiber (**Fig. 6a**). Cortical responses to light-stimuli were measured shortly after surgery (30-60 min) and 1, 4 and 7 days after the Ziapin2 injection. Ziapin2 fluorescence analyzed in brain slices showed a diffusion diameter in the range of 1 mm and persisted up to 7 days from injection (**Fig. 6b**). Immunohistochemistry in cortical slices at the injection site performed 7 days after the injection demonstrated that Ziapin2 did not alter the inflammatory reaction to the surgery, as evaluated by the expression of GFAP and Iba1, specific markers for astrocytes and microglia, respectively (**Fig. S18**). Optical stimulation at various power densities induced activation of cortical activity evaluated as extracellular local field potentials (LFPs) that peaked at about 200 ms after light-onset (**Fig. 6c**). Ziapin2 induced a significant dose-dependent increase in the LFP amplitude with respect to vehicle-injected animals that was more pronounced for 200 ms stimuli (**Fig. 6d**). Analysis of the time-course of the light-evoked LFP responses revealed that the optical stimulation of cortical activity persisted up to 7 days after injection (**Fig. 6e,f**).

Conclusions

We report here on a new opto-mechanical effect driven by intramembrane molecular machines composed of clustered photochromic molecules. The predictions by MD simulations, confirmed by experimental observations on artificial membranes, are consistent with a model in which the hydrophobic azepane-substituted aniline in the amphiphilic azobenzenes on the two sides of the membrane interact when in *trans* configuration, retracting to *cis* after photoconversion. This brings about shrinkage of the membrane upon *trans* Ziapin2 loading, that eventually relaxes to the natural thickness following light-induced Ziapin2 dissociation. The evoked relaxation increases membrane thickness, thus transiently decreasing its capacitance.

Ziapin2 differentiates from previously reported capacitance-changing azobenzene-cored amphiphilic probes containing long alkyl chains (6-8, 35,36) for distinctive functional groups and features, namely: (i) the two hexyl chains ω-terminated with pyridinium bromide that target the membrane (35,36); (ii) the presence of an amine on both azobenzene sides that, as strong electron-donor group, red-shifts azobenzene absorption to the visible; (iii) the azepane moiety that mediates the formation of *trans*-Ziapin2 dimers through the interaction between two facing Ziapin2 molecules on opposite bilayer leaflets. Thanks to these features, Ziapin2 responds to millisecond range visible light stimuli by deforming the membrane and causing the fast physiological effects.

The light-induced capacitance drop generates a pure capacitive current responsible for a hyperpolarizing shift that depends on membrane coverage and rate of capacitance change. These effects do not involve ion channels, being recapitulated by Hek293 cells and neurons subjected to intra/extracellular blockade of membrane conductances. Thus, we are exploiting a novel membrane nanomachine with a mechanical effect at the molecular scale.

Although the existence of lipid rafts is a matter of controversy (37), photochromic molecules have been already targeted to lipid rafts (38). The propensity of Ziapin2 to localize to cholesterol and sphingolipid-enriched membrane microdomains is functionally important. Indeed, the membrane thinning effect, evaluated by AFM, was amplified in raft-like bilayers, and disruption of lipid rafts caused disappearance of Ziapin2 clusters and decrease of light-induced hyperpolarization.

Several papers reported a link between temperature-dependent decrease in membrane thickness, increased capacitance and depolarization (22-25), demonstrating that membrane capacitance is effective in modulating neuronal activity. In the dark, Ziapin2-induced increase in capacitance renders neurons less excitable and more refractory to membrane-voltage changes. This stabilization of neuronal activity is a potentially exploitable effect in the regulation of network excitability and in demarcating the discharge areas in neuronal networks. In response to light stimulation, Ziapin2 controls AP firing through two cooperating mechanisms: (i) the fast light-induced C_m decrease, generating hyperpolarization, followed by a slower C_m increase at the light offset, associated with rebound depolarization, as predicted by the equivalent circuit simulation; (ii) membrane hyperpolarization may cause an "*anode break excitation*" at the light-offset, decreasing outward K^+ current and removing Na^+ channel inactivation (39). The rebound post-hyperpolarization AP firing depends on the duration of membrane hyperpolarization (40), explaining the limitation in the maximal stimulation frequency that can be achieved.

Neurons display larger depolarization, with respect to Hek293 cells, that is sensitive to synaptic transmission, which instead does not affect hyperpolarization. Depolarization may contribute to the light-evoked firing through a positive feedback within the network mediated by excitatory synaptic transmission. In this respect, using conjugated polymer interfaces, we previously showed that light-induced inhibition is followed by a rebound depolarization and firing (19,23), indicating that the fast return of capacitance and voltage to basal levels is responsible for neuronal activation.

With respect to optogenetic light-gated ion channels such as ChETA, Ziapin2 does not interfere with ionic fluxes or reversal potential of membrane conductances, but directly targets passive membrane properties. Although the Ziapin2 effect is slower than that of a light-driven ion channel, it has a comparable ability in eliciting of APs.

Ziapin2 is not harmful to primary neurons, and neuronal activation by Ziapin2 is persistent *in vitro*, in spite of the slow decrease of the plasma membrane concentration due to membrane turnover. Moreover, Ziapin2 is effective in inducing a light-dependent electrical activation of the cortical

networks after *in vivo* injection in the somatosensory cortex of the mouse, with a sustained effect of photostimulation and a complete absence of inflammatory responses to the compound, paving the way to their potential future *in vivo* applications.

In conclusion, our new amphiphilic photochromic molecules have several characteristics that differentiate them from previous compounds, namely: (i) marked affinity for the hydrophobic environment of the membrane; (ii) high tolerability and sensitivity to the visible spectrum; (iii) reversible photoinduction of local membrane deformations altering membrane capacitance, potential and firing in the absence of heat generation; (iv) effectiveness and prolonged effects *in vivo*. In view of these features, these molecules display a high potential for future applications in neurosciences and biomedicine.

Acknowledgements. We thank drs. Floriana Fruscione and Federico Zara (Giannina Gaslini Institute, Genova, Italy) for help in preparing iPSC-derived human neurons; drs. Paolo Bianchini, Michele Oneto and Marco Scotto (Center for Nanoscopy and Nikon Imaging Center, Istituto Italiano di Tecnologia, Genova, Italy); dr. Lorenzo Cingolani (Center for Synaptic Neuroscience and Technology, Istituto Italiano di Tecnologia, Genova, Italy) for providing the ChETA-encoding lentiviral vectors; drs. Arta Mehilli and Giulia Mantero (Center for Synaptic Neuroscience and Technology, Istituto Italiano di Tecnologia, Genova, Italy) for precious help in primary cultures and *in vivo* elelectrophysiology, respectively. This work was supported by the Italian Ministry of Health (project RF-2013-02358313 to GP, GL and FB) and Istituto Italiano di Tecnologia (pre-startup project to GL and FB). The support of the Ra.Mo. Foundation (Milano, Italy), Fondazione 13 Marzo (Parma, Italy), Rare Partners srl (Milano, Italy) and Fondazione Cariplo (project 2018-0505) to GL and FB are also acknowledged.

Author contributions. C.B. designed and engineered Ziapin2. S.C., L.C. and F.O. performed the synthesis and characterization of Ziapin2. D.F. calculated the atomic charges and optimized

coordinates. G.M.P. performed the spectroscopic characterization. L.M. performed molecular dynamics simulations. M.D.S., L.L. and M.M. performed planar lipid membrane and AFM studies. M.B., G.G. and E.C. studied the *in vitro* and *in vivo* distribution of the Ziapin compounds in neurons. M.L.D., P.B., E.C. and F.L. performed the in vitro patch-clamp experiments and analyzed the data. V.V. elaborated the numerical RC model. J.F. M-V., E.C., D.S. and C.G.E. performed and analyzed the *in vivo* experiments. M.L.D., E.C., P.B., G.M.P. and F.L. contributed to paper writing. G.L., C.B. and F.B. conceived the work, G.L. and F.B. planned the experiments, analyzed the data and wrote the manuscript.

Competing interests. The authors declare no competing interests.

Additional information. Supplementary information is available for this paper.

Data availability statement. The datasets generated and analyzed during the current study are available from the corresponding author on reasonable request.

REFERENCES

1. Paoletti P, Ellis-Davies GCR, Mourot A. Optical control of neuronal ion channels and receptors. *Nat Rev Neurosci* 20: 514-532 (2019).

2. Rivnay J, Wang H, Fenno L, Deisseroth K, Malliaras G. Next-generation probes, particles, and proteins for neural interfacing. *Sci Adv* 3: e1601649 (2017).

3. Tønnesen J. Optogenetic cell control in experimental models of neurological disorders. *Behav Brain Res* 255: 35-43 (2013).

4. Deisseroth K Optogenetics: 10 years of microbial opsins in neuroscience. *Nat Neurosci* 18: 1213-1225 (2015).

5. Zhang JJ, Wang JX, Tia H. Taking orders from light: progress in photochromic bio-materials. *Mater Horizons* 1: 169-184 (2014).

6. Fujiwara H, Yonezawa Y, Photoelectric response of a black lipid membrane containing an amphiphilic azobenzene derivative. *Nature* 351: 724-726 (1991).

7. Yonezawa Y, Fujiwara H, Sato T. Photoelectric response of black lipid membranes incorporating an amphiphilic azobenzene derivative. *Thin Solid Films* 210/211: 736-738 (1992).

8. Tanaka M, Yonezawa Y. Photochemical regulation of ion transport through “quasi-channels” embedded in black lipid membrane. *Mat Sci Engineer C* 4: 297-301 (1997).

9. Garner LE, Park J, Dyar SM, Chworos A, Sumner JJ, Bazan GC. Modification of the optoelectronic properties of membranes via insertion of amphiphilic phenylenevinylene oligoelectrolytes. *JACS* 132: 10042-10052 (2010).

10. Hinks J, Wang Y,Han Poh W, Donose B C, Thomas A W, Wuertz S, Loo S C J, Bazan G C, Kjelleberg S, Mu Y, Seviour T. Modeling cell membrane perturbation by molecules designed for transmembrane electron transfer. *Langmuir* 30: 2429−2440 (2014).

11. Gorostiza P, Isacoff E. Optical switches and triggers for the manipulation of ion channels and pores. *Mol Biosyst* 3: 686-704 (2007).

12. Fortin DL, Banghart MR, Dunn TW, Borges K, Wagenaar DA, Gaudry Q, Karakossian MH, Otis TS, Kristan WB, Trauner D, Kramer RH. Photochemical control of endogenous ion channels and cellular excitability. *Nat Methods* 5: 331-338 (2008).

13. Kramer RH, Mourot A, Adesnik H. Optogenetic pharmacology for control of native neuronal signaling proteins. *Nat Neurosci* 16: 816-823 (2013).

14. Tochitsky I, Kienzler MA, Isacoff E, Kramer RH. Restoring vision to the blind with chemical photoswitches. *Chem Rev* 118: 10748-10773 (2018).

15. Laprell L, Hüll K, Stawski P, Schön C, Michalakis S, Biel M, Sumser MP, Trauner D. Restoring light sensitivity in blind retinae using a photochromic AMPA receptor agonist. *ACS Chem Neurosci* 7: 15-20 (2016).

16. Laprell L, Tochitsky I, Kaur K, Manookin MB, Stein M, Barber DM, Schön C, Michalakis S, Biel M, Kramer RH, Sumser MP, Trauner D, Van Gelder RN. Photopharmacological control of bipolar cells restores visual function in blind mice. *J Clin Invest* 127: 2598-2611 (2017).

17. Ghezzi D, Antognazza MR, Dal Maschio M, Lanzarini E, Benfenati F, Lanzani G. A hybrid bioorganic interface for neuronal photoactivation. *Nat Commun* 2: 166 (2011).

18. Ghezzi D, Antognazza MR, Maccarone R, Bellani S, Lanzarini E, Martino N, Mete M, Pertile G, Bisti S, Lanzani G, Benfenati F. A polymer optoelectronic interface restores light sensitivity in blind rat retinas. *Nat Photonics* 7: 400-406 (2013).

19. Feyen P, Colombo E, Endeman D, Nova M, Laudato L, Martino N, Antognazza MR, Lanzani G, Benfenati F, Ghezzi D. Light-evoked hyperpolarization and silencing of neurons by conjugated polymers. *Sci Rep* 6: 22718 (2016).

10. Rand D, Jakešová M, Lubin G, Vėbraitė I, David-Pur M, Đerek V, Cramer T, Sariciftci NS, Hanein Y, Głowacki ED. Direct electrical neurostimulation with organic pigment photocapacitors. *Adv Mater* 30: e1707292 (2018).

21. Maya-Vetencourt JF, Ghezzi D, Antognazza MR, Colombo E, Mete M, Feyen P, Desii A, Buschiazzo A, Di Paolo M, Di Marco S, Ticconi F, Emionite L, Shmal D, Marini C, Donelli I, Freddi G, Maccarone R, Bisti S, Sambuceti G, Pertile G, Lanzani G, Benfenati F. A fully organic retinal prosthesis restores vision in a rat model of degenerative blindness. *Nat Mater* 16: 681-689 (2017).

22. Martino N, Feyen P, Porro M, Bossio C, Zucchetti E, Ghezzi D, Benfenati F, Lanzani G, Antognazza MR. Photothermal cellular stimulation in functional bio-polymer interfaces. *Sci Rep* 5: 8911 (2015).

23. Lodola F, Martino N, Tullii G, Lanzani G, Antognazza MR. Conjugated polymers mediate effective activation of the mammalian ion channel transient receptor potential vanilloid 1. *Sci Rep* 7: 8477 (2017).

24. Shapiro MG, Homma K, Villarreal S, Richter CP, Bezanilla F. Infrared light excites cells by changing their electrical capacitance. *Nat Commun* 3: 736 (2012).

25. Carvalho-de-Souza JL, Treger JS, Dang B, Kent SB, Pepperberg DR, Bezanilla F. Photosensitivity of neurons enabled by cell-targeted gold nanoparticles. *Neuron* 86: 207-217 (2015).

26. Bandara HM, Burdette SC. Photoisomerization in different classes of azobenzene. *Chem Soc Rev* 41: 1809-1825 (2012).

27. Hartley GS. The Cis-form of Azobenzene. Nature 140: 281-281 (1937).

28. Rau H. Spectroscopic properties of organic azo compounds. *Angewandte Chemie* 12: 224-235 (1973).

29. Tang BZ, Qin A. *Aggregation-induced emission: fundamentals.* John Wiley & Sons (2013).

30. Sierocki P, Maas H, Dragut P, Richardt G, Voegtle F, De Cola L, Brouwer F, Zink JI. Photoisomerization of azobenzene derivatives in nanostructured silica. *J Phys Chem B* 110: 24390-24398 (2006).

31. Fendler JH. Surfactant vesicles as membrane mimetic agents: characterization and utilization. *Acc Chem Res13*: 7-13 (1980).

32. Head BP, Patel HH, Insel PA. Interaction of membrane/lipid rafts with the cytoskeleton: impact on signaling and function: membrane/lipid rafts, mediators of cytoskeletal arrangement and cell signaling. *Biochim Biophys Acta* 1838: 532-545 (2014).

33. Fruscione F, Valente P, Sterlini B, Romei A, Baldassari S, Fadda M, Prestigio C, Giansante G, Sartorelli J, Rossi P, Rubio A, Gambardella A, Nieus T, Broccoli V, Fassio A, Baldelli P, Corradi A, Zara F, Benfenati F. PRRT2 controls neuronal excitability by negatively modulating Na^+ channel 1.2/1.6 activity. *Brain* 141: 1000-1016 (2018).

34. Thalhammer A, Contestabile A, Ermolyuk YS, Ng T, Volynski KE, Soong TW, Goda Y, Cingolani LA. Alternative splicing of P/Q-type Ca^{2+} channels shapes presynaptic plasticity. *Cell Rep* 20: 333-343 (2017).

35. Zhang Q, Bazuin CG. Liquid crystallinity and other properties in complexes of cationic azo-containing surfactomesogens with poly(styrenesulfonate). *Macromolecules* 42: 4775-4786 (2009).

36. Peddie V, Anderson J, Harvey JE, Smith GJ, Kay A. Synthesis and solution aggregation studies of a suite of mixed neutral and zwitterionic chromophores for second-order nonlinear optics. *J Org Chem* 79: 10153-10169 (2014).

37. Allen JA, Halverson-Tamboli RA, Rasenick MM. Lipid raft microdomains and neurotransmitter signalling. *Nat Rev Neurosci* 8: 128-140 (2007).

38. Frank JA, Franquelim HG, Schwille P, Trauner D. Optical control of lipid rafts with photoswitchable ceramides. *J Am Chem Soc* 138: 12981-12986 (2016).

39. Hodgkin Al, Huxley AF. A quantitative description of membrane current and its application to conduction and excitation in nerve. *J Physiol* 117: 500 -544 (1952).

40. Tremere LA, Pinaud R, Irwin RP, Allen CN. Postinhibitory rebound spikes are modulated by the history of membrane hyperpolarization in the SCN. *Eur J Neurosci* 28: 1127-1135 (2008).

41. Jo S, Kim T, Iyer VG, Im W. CHARMM-GUI: A Web-based Graphical User Interface for CHARMM. *J Comput Chem* 29:1859-1865 (2008).

42. Phillips JC, Braun R, Wang W, Gumbart J, Tajkhorshid E, Villa E, Chipot C, Skeel RD, Kalé L, Schulten K. Scalable molecular dynamics with NAMD +. *J Comput Chem.* 26: 1781-1802 (2005).

43. Huang J, MacKerell AD Jr. CHARMM36 all-atom additive protein force field: validation based on comparison to NMR data. *J Comput Chem* 34: 2135-2145 (2013).

44. Bennett WF, Tieleman DP. Molecular simulation of rapid translocation of cholesterol, diacylglycerol, and ceramide in model raft and nonraft membranes. *J Lipid Res* 53: 421-429 (2012).

528 45. Maragliano L, Vanden-Eijnden E. A temperature accelerated method for sampling free energy and
529 determining reaction pathways in rare events simulations. *Chem Phys Lett* 426: 168-175 (2006).
530
531 46. Dalla Serra M, Menestrina G. Liposomes in study of pore-forming toxins. *Meth Enzymol* 372: 99-
532 124 (2003).
533
534 47. Dalla Serra M, Menestrina G Characterization of molecular properties of pore forming toxins with
535 planar lipid bilayers. *Meth Mol Biol* 145: 171-188 (2000).
536
537 48. Schmitt BM, Koepsell H. An improved method for real-time monitoring of membrane capacitance
538 in Xenopus laevis oocytes. *Biophys J* 82: 1345 1357 (2002).
539
540 49. Pusch M, Neher E. Rates of diffusional exchange between small cells and a measuring patch
541 pipette. *Pflugers Arch* 411: 204-211 (1988).
542
543 50. Gillis KD. Admittance-based measurement of membrane capacitance using the EPC-9 patch-
544 clamp amplifier. *Pflugers Arch* 439: 655-664 (2000).
545
546
547
548

FIGURE LEGENDS

Figure 1. *Trans→cis* isomerisation of Ziapin2 in various environments

(**a**) Schematics of the isomerisation process in Ziapin2. (**b,c**) Changes in the Ziapin2 absorbance spectrum (25 μM in DMSO) as a function of time (**b**) and time-course of absorbance at 450 nm upon illumination with a diode laser (**c**). The collective photoswitching dynamics upon light exposure, reveals a well-defined and relatively fast photoreaction dynamics of Ziapin2 in DMSO, reaching a photostationary population after about 100 s of illumination and achieving a complete recovery with a $t_{1/2}$ of 108 s in the dark at room temperature. While the photoisomerisation process occurs typically in the picosecond range, the population dynamics toward the photostationary state takes much longer, depending on the conformer thermodynamic stability and molecular environment. (**d,e**) Changes in the Ziapin2 PL spectrum (25 μM in DMSO) as a function of time (**d**) and time course of the emission at 540 nm upon excitation at 450 nm with a Xenon lamp (**e**). The red line is the numerical model employed to describe the time-evolution of the fluorescence signal. (**f**) Photoswitching/relaxation dynamics of Ziapin2 in DMSO, Hek293 cells and water acquired by exciting at 450 nm and collecting the emission at 540, 580 and 620 nm, respectively. (**g**) Zoom on the PL dynamics in Hek293 cells, highlighting the stretched exponential decay. Such function takes into account the distribution of relaxation times occurring in disordered environments.

Figure 2. Ziapin2 distributes to the plasma membrane and lipid rafts in neurons

(a) Snapshots extracted from an MD simulation showing Ziapin2 (*trans*) spontaneously entering the membrane (PC lipid model) at consecutive time frames (I-IV); lipid phosphate atoms are shown as orange spheres, and acyl chains as grey lines; water molecules are not reported for clarity. **(b)** Time dependence of the distance between the center of mass (COM) of Ziapin2 and the bilayer center in three independent simulations; the dashed line indicates the interface between water and lipid head groups. **(c)** Free Energy profile for Ziapin2 (*trans*) entering the membrane bilayer, calculated versus

575 the distance between the bilayer center and the center of mass of the two pyridinic nitrogens of
576 Ziapin2. **(d)** Primary neurons pulse exposed to Ziapin2 for 7 min were stained with the specific plasma
577 membrane reporter Cell Mask (red) to evaluate the membrane incorporation of Ziapin2 (green). Scale
578 bars: (**d**) 10 and 20 μm for large and small panels, respectively. **(e)** Primary neurons pulse exposed to
579 Ziapin2 (green) for 7 min were stained with the specific lipid raft marker Vybrant™ Alexa Fluor™ 555
580 (red) with or without pretreatment with methyl-β-cyclodextrin (MβCD) to deplete cholesterol and
581 imaged by Structured Illumination Microscopy (SIM). Scale bars: 5 and 2 μm for large and small
582 panels, respectively. **(f)** Analysis of z-stack confocal images of Cell Mask/Ziapin2 and Vybrant/Ziapin2
583 double-stained neurons. *Upper panel:* Partitioning of Ziapin2 to the plasma membrane and lipid rafts
584 was evaluated as the percentage of total cell Ziapin2 fluorescence colocalizing with the respective
585 marker 7 min after loading and subsequent washout. Means ± sem with individual experimental points
586 are shown. *Lower panel:* Percentage of the total plasma membrane (Cell Mask staining) or lipid raft
587 domains (Vybrant staining) that were positive for Ziapin2 7 min after loading. Means ± sem with
588 individual experimental points are shown. The Vibrant/Cell Mask surface ratio, determined in parallel
589 samples double labeled with the two probes was 71 ± 2%. **p<0.01; ***p<0.001, unpaired Student's *t*-
590 test (n = 26 and 39 for Cell Mask and Vybrant staining, respectively, from 3 independent primary
591 neuronal preparations). **(g)** Effects of cholesterol depletion on the membrane distribution of Ziapin2.
592 Representative images of Ziapin2 clusters acquired by SIM imaging in control neurons and neurons
593 pretreated with MβCD. Scale bars: 2 μm. The line-scan fluorescence intensity plots reveal a dot-
594 pattern profile for Ctrl samples (black traces) and a more diffuse signal for MβCD-treated cells (red
595 traces). **(h)** The density of Ziapin2 clusters and of Vybrant-labeled rafts (puncta/μm^2) and their
596 average size were evaluated washout in untreated (Ctrl) and MβCD-treated neurons after 7 min of
597 Ziapin2 labeling and subsequent live staining with Vybrant to label lipid rafts. Means ± sem with
598 individual experimental points are shown. **p<0.01; ***p<0.001, Kruskal-Wallis/Dunn's test (n = 20 for
599 Ctrl and MβCD, respectively, from 3 independent neuronal preparations).
600

Figure 3. Ziapin2 reversibly modifies membrane thickness in artificial membranes, cell lines and neurons

(a) *Upper panels:* Average membrane thickness maps, shown perpendicular to the bilayer plane, for the simulations of Ziapin2 (8 molecules) in *trans* (left) and *cis* (right) conformations, respectively. Ziapin2 molecules were embedded in phosphatidylcholine (PC) model membranes. For the two Ziapin2 conformations, simulations (200 ns/trajectory) were started with the molecule in the equilibrium position. In both cases, the position along the bilayer normal was stationary over the whole trajectory, while the orientation fluctuated between a parallel and a perpendicular state. Axis and thickness values are in Å. *Lower panels:* Snapshots from simulations of Ziapin2 (8 molecules) in *trans* (left) and *cis* (right) conformations, respectively. **(b)** *Upper panels:* Average thickness maps of a raft membrane model (simulations with 8 Ziapin2 molecules in *trans* (left) and *cis* (right) conformations, respectively). The raft membrane model is composed of a mixture of PC, SM and cholesterol (CHO) (1:1:1). Axis and thickness values are in Å. *Lower panels:* Snapshots from the simulations of 8 Ziapin2 molecules in *trans* (left) and *cis* (right) conformations. PC lipid molecules are shown as grey lines, and phosphate atoms as orange spheres; cholesterol and SM molecules are shown as red and blue lines, respectively; water molecules and ions are not reported for clarity. **(c)** AFM maps realized in liquid environment on lipid bilayers formed either by PC (top) or PC:SM:CHO (bottom) on mica and exposed to Ziapin2 or DMSO. Maps of Ziapin2-containing bilayers show the spatial distribution of depressed areas and the fine structure of the roughness modulation (left and middle panels at different magnification), while DMSO containing bilayers show a very well preserved uniformity (right). **(d)** *Top*: Bilayer thickness after Ziapin2 incorporation in the dark with respect to the untreated nominal value (broken line). *Bottom:* Ratio between the area of depressed membrane and the total lipid-covered area. Raft-like bilayers show a higher decrease in thickness (top) and a more extended area of depression (bottom) when exposed to Ziapin2 if compared with single PC bilayers. The effects of Ziapin2 on thickness and depressed area are statistically significant for both types of bilayer ($p<0.05$ for both PC and PC:SM:CHO, one sample Student *t*-test) and significantly more pronounced in raft-

like than in pure PC membranes (***p<0.001, Mann-Whitney *U*-test, n = 7 and 9 for PC and PC:SM:CHO, respectively). **(e)** Planar lipid membrane experiments realized with PC (left) or PC:SM:CHO (right) show a systematic increase of capacitance measured across the bilayers when Ziapin2 was present in both recording chambers with respect to the sole insertion in one of the two sides. *p<0.05, Mann-Whitney *U*-test (n = 6 and 5 for Ziapin2 and DMSO, respectively for each type of bilayer). **(f)** Evaluation of cell capacitance changes (means ± sem) by patch-clamp recordings after exposure of Hek293 cells to either DMSO (0.25% v/v; black) or Ziapin2 (5 µM in DMSO; red) in the dark. °°°p<0.001, Mann Whitney *U*-test (n = 8 and 9 for DMSO and Ziapin2, respectively).

Figure 4. Light-evoked membrane voltage modulation by Ziapin2 in primary neurons

(a) Primary hippocampal neurons at 14 DIV were incubated with Ziapin2 for 7 min, washed and recorded by whole-cell patch-clamp either immediately after pulse labeling or 7 days after. Scale bar, 20 µm. **(b)** *Left:* Representative averaged capacitance traces of neurons pulse labeled with either DMSO (0.25% v/v; black traces) or Ziapin2 (5 µM in DMSO; red traces), washed and recorded in current-clamp configuration in the presence of synaptic blockers before and after light stimulation (470 nm; 18 mW/mm^2; cyan-shaded areas). In the bottom panel, single cell correlation between the capacitance increase in the dark upon Ziapin2 addition (X-axis) and the phasic capacitance drop induced by light (Y-axis). Pearson's correlation coefficient -0.801, p<0.05. *Right:* Box plots of the peak capacitance changes after exposure of neurons to either DMSO (0.25% v/v; black) or Ziapin2 (5 µM in DMSO; red) in the dark (DMSO, n=11; Ziapin2, n=13) and subsequent illumination in the presence of the compound and of synaptic blockers. The same neurons were recorded under basal conditions, added with either DMSO or Ziapin2 and finally stimulated with light. **p<0.01; ***p<0.001; Ziapin2 *vs* DMSO, Friedman/Dunn's tests. **(c)** Representative whole-cell current-clamp traces recorded from neurons incubated with either 0.25% (v/v) DMSO (black traces) or 5 µM Ziapin2 in DMSO (red traces) in the absence (Ctrl) or presence of synaptic blockers (SB; see Materials and Methods), and after 7 days of incubation in the presence of synaptic blockers. The duration of the light stimulation (20 and

200 ms) is shown as a cyan-shaded area (470 nm; 18 mW/mm^2). In the insets, traces are shown in an expanded time scale. **(d)** Box plots of the peak hyperpolarization (left) and peak depolarization (right) changes in primary neurons exposed to DMSO/Ziapin2 and subjected to 20/200 ms light stimulation in the absence (Ctrl) or presence of synaptic blockers. Hyperpolarization and depolarization were measured as the minimum and maximum voltage, respectively, reached within 350 ms from light-onset. The box plots show that the peak hyperpolarization response generated by the presence of Ziapin2 is an intrinsic response of the neuron and is not affected by the presence of blockers of synaptic transmission, while depolarization, already present in synaptically isolated neurons, is enhanced by active synaptic transmission. **(e)** Time-to-peak hyperpolarization, depolarization and capacitance changes as a function of the light stimulus duration under Ctrl and synaptic block conditions. Data (means ± sem) represent the time necessary to reach the minimum and maximum membrane voltages in the above-mentioned time windows. **(f)** Persistence of the light response over time. The residual light-induced hyperpolarization (*left*) and depolarization (*right*) effects observed 7 days after the initial Ziapin2 loading in the presence of synaptic blockers are expressed in percentage of the corresponding effects measured acutely after Ziapin2 loading. Box plots are shown for both 20 and 200 ms light stimuli. All experiments with neurons were carried out at 24 ± 1 °C. *p<0.05; **p<0.01; ***p<0.001 DMSO *vs* Ziapin2, Mann Whitney *U*-test. Ziapin2-treated neurons: n = 19, 20, 15 (20 ms) and n = 20, 19, 14 (200 ms) for Ctrl, SB and 7d/SB, respectively; DMSO-treated neurons: Ctrl, SB, 7d/SB: n = 10, 7, 10 for both 20 and 200 ms.

Figure 5. Light-evoked firing activity in primary neurons loaded with Ziapin2

(**a-c**) Representative averaged traces recorded in current-clamp configuration from neurons incubated with either DMSO (0.25% v/v, black traces) or Ziapin2 (5 μM in DMSO, red traces) in the absence (**a**; Ctrl) or presence of synaptic blockers (**b**). In (**c**) recordings were performed 7 days after Ziapin2 labeling with synaptic blockers. Light stimulation (470 nm; 18 mW/mm^2) is shown as a cyan-shaded area. (**d-f**) Peristimulus time histograms (PSTHs; bin=20 ms) reconstructed from the firing rate of

neurons recorded in the absence (**d**) or presence of synaptic blockers 7 min (**e**) and 7 days (**f**) after DMSO /Ziapin2 labeling, respectively and subjected to either 20 ms (upper panel) or 200 ms (lower panel) light stimulation. Ziapin2-treated neurons: n = 7, 11, 5 (20 ms) and n = 6, 10, 4 (200 ms) for Ctrl, synaptic blockers, 7d/synaptic blockers, respectively; DMSO-treated neurons: n = 4, 7, 10 (20 and 200 ms) for Ctrl, synaptic blockers, 7d/synaptic blockers, respectively. *p<0.05; **p<0.01; ***p<0.001 DMSO *vs* Ziapin2, Mann-Whitney *U*-test on 160 ms bins (20 ms stimulation) and 240 ms bins (200 ms stimulation). **(g)** PSTH areas of AP firing in response to 20/200 ms light stimulation in the presence of synaptic blockers recorded either acutely or 7 days after Ziapin2 exposure. N=10 (acute); N=5 (7 days); ns, not significant, Mann Whitney *U*-test. **(h)** Representative AP firing activities recorded from neurons incubated with Ziapin2 (5 µM) in the absence of synaptic blockers and stimulated with 200 ms light pulses administered at 1 Hz (upper traces) or with 20 ms light pulses administered at 5 Hz (lower traces). **(i)** *Left:* Representative phase plane plot analysis of AP waveforms generated in the same Ziapin2-loaded neuron before (grey trace) and after (blue trace) light stimulation (470 nm; 20 ms pulses @ 20 mW/mm^2). *Right:* Quantification of the maximal rising and repolarizing slopes and of the AP peak amplitude before and after illumination. *p<0.05; **p<0.01, paired Student's *t*-test (n=7 neurons).

Fig. 6. Light-evoked cortical responses *in vivo* in mice loaded with Ziapin2 in the somatosensory cortex

(a) Schematic representation of the stereotaxic injection of Ziapin2 (200 µM in 1 µl 10% DMSO) in the somatosensory cortex (S1ShNc, 2 mm anterior to lambda, 2 mm lateral to midline, and – 723 µm ventral to brain surface) and of the 16-microelectrode array implant for local field potential (LFP) recordings coupled with optical fiber for photostimulation. **(b)** Bright field image (left) and endogenous LC339 fluorescence micrograph (right) of unfixed slices from the injected somatosensory cortex taken 1, 4 and 7 days after Ziapin2 administration. The injection site and the diffusion of the compound are visible. Scale bar, 150 µm. **(c)** Representative recordings of LFPs evoked in the somatosensory cortex

by 20 and 200 ms light stimulation (43 mW/mm^2) in mice injected with either DMSO (black trace) or Ziapin2 (red trace) 1 day before. The cyan-shaded areas represent the light stimulation. Potentials were considered significant above 2-fold the standard deviation range (broken horizontal lines). **(d)** Dose-response analysis of LFP responses in DMSO- (black) or Ziapin2- (red) injected mice as a function of power and duration of the light stimulus (20 and 200 ms; open and closed symbols, respectively). The peak amplitude of light evoked LFPs was normalized by the averaged noise amplitude calculated from the non-responding channels over the same epoch. Photostimulation at increasing power from 4 to 116 mW/mm^2 triggered significant responses in Ziapin2-injected animals that were already significant at 25 mW/mm^2 (200 ms stimulus). No significant responses were recorded in DMSO-treated animals. **(e,f)** Time-course of the normalized LFP amplitude recorded in the somatosensory cortex 1, 4 and 7 days after intracortical injection of either DMSO (black) or Ziapin2 (red). LFPs were evoked by 20 (open symbols) and 200 (closed symbols) ms light stimuli at 43 (**e**) and 116 (**f**) mW/mm^2. 20 ms: $^{xx}p<0.01$, $^{xxx}p<0.001$; 200 ms: °°p<0.01; °°°p<0.001; repeated measure ANOVA/Tuckey's tests *vs* DMSO-injected control (n=3 mice for each experimental group).

ONLINE METHODS

Synthesis and characterization of Ziapin2. The synthetic route consists in the reduction of the nitro group of the Disperse Dye Orange 3 in amine, which is then alkylated with α,ω-dibromohexane and finally treated with pyridine to yield the terminated pyridinium bromide.

Unless otherwise stated, all chemicals and solvent were commercially available and used without further purification. Thin layer chromatography (TLC) was performed using silica gel on aluminum foil (Sigma Aldrich). ^{1}H and ^{13}C NMR spectra were collected with a Bruker ARX400. Mass spectroscopy was carried out with a Bruker Esquire 3000 plus.

4-[2-(4-aminophenyl)diazen-1-yl]aniline (1)

A mixture of Disperse Orange 3 (Sigma Aldrich, 1.21 g, 5.0 mmol) and $Na_2S \cdot 9H_2O$ (3.60 g 15.0 mmol) dissolved in 100 mL of MeOH is refluxed overnight under stirring. Then the mixture is cooled to room temperature and the solvent is removed under reduced pressure. The resulting red powder is washed with DCM and Et_2O, the combined organic layers are collected, and the solvent is evaporated under reduced pressure, to give 540 mg of the desired product **1** as an orange powder in 51% yield.

^{1}H NMR: (400MHz, DMSO) δ 7.56 (d, J= 8.82Hz, 2H), 6.62 (d, J=8.82Hz, 2H), 5.70 (s, 4H)

4,4'-Bis-(N,N-di-ω-bromohexyl)diaminoazobenzene (Azo-Br4), Azo-Br1, Azo-Br2.

537 mg of **1** (2.53 mmol) is stirred in 10 ml of previously degassed acetonitrile. 2.20 g of K_2CO_3 (15.9 mmol) and 1.6 ml of 1,6-dibromohexane (10.4 mmol) are added dropwise to the reaction mixture and refluxed for 72 hours, while monitored by TLC. The reaction mixture is filtered and the solid is washed three times with diethyl ether, ethylacetate and dichloromethane. The excess of dibromohexane is removed under reduced pressure (3 10^{-1} mbar) at 70 °C. The raw material is purified by flash chromatography with silica gel using hexane: Et_2O 3:1 as eluent to give 52 mg of 4,4'-Bis-(N,N-di-ω-bromohexyl)diaminoazobenzene (Azo-Br4, 2.4 % yield), 32 mg of Azo-Br1 (2.8 % yield) and 33 mg Azo-Br2 (2.1 % yield) are also recovered.

Azo-Br4: 1H-NMR: (400MHz, DMSO) δ (ppm) 7.62 (d, J= 8.80 Hz, 4H), 6.72 (d, J=8.80 Hz, 4H), 3.53

(t, 16H), 1.82 (m, 8H), 1.56 (m, -CH_2-,8H), 1.44 (m, -CH_2-,8H), 1.35 (m, -CH_2-, 8H); MS : 865 $(M + H)^+$, 887 $(M + Na)^+$

Azo-Br1: 1H-NMR: (400MHz, DMSO) δ (ppm) 7.63 (d, J= 8.80Hz, 2H), 7.58 (d, J= 8.80 Hz, 2H), 6.77 (d, J= 8.80Hz, 2H), 6.64 (d, J= 8.80Hz, 2H), 6.21 (t, -NH, 1H), 3.54 (t, -N-CH_2-, 6H), 3.09 (m, CH_2-NH, 2H), 1.83-1.42 (m, 1 CH_2-, 6H); MS: 458 $(M + H)^+$

Azo-Br2: 1H-NMR: (400MHz, DMSO) δ (ppm) 7.63 (d, J= 8.80Hz, 4H), 6.77 (d, J= 8.80 Hz, 2H), 6.72 (d, J= 8.80Hz, 2H), 3.53 (t, -N-CH_2-, 8H), 3.35 (t, -CH_2-Br), 1.82-1.35 (m, -CH_2-, 24H); MS : 621 $(M + H)^+$

1-{6-[(4-{2-[4-(azepan-1-yl) phenyl]diazen-1-yl}phenyl)[6-(pyridin-1-ium-1-yl) hexyl] amino] hexyl} pyridin-1-ium dibromide (Ziapin 2)

12 mg of **Azo-Br2** are dissolved in 3 ml of pyridine and stirred at room temperature for 42 hrs. Then 3 ml of methanol are added and further stirred for 60 hrs. The excess of pyridine and methanol are removed from the reaction mixture under reduced pressure to give a solid in quantitative yield that is further washed with small portions of hexane.

^{1}H NMR: (400MHz, DMSO) δ 9.09 (d, Pyr, 4H), 8.61 (t, Pyr, 2H), 8.16 (t, Pyr, 4H), 7.62 (d, J= 8.8 Hz, Ph, 4H), 6.78 (d, J=8.8 Hz, Ph, 2H), 6.70 (d, J= 8.8 Hz, Ph, 2H), 4.60 (t, -CH_2-Pyr-, 4H), 3.54 (t, N-CH_2-, 4H), 2.97-1.24 (m, 24H). ^{13}C NMR: (400 MHz, DMSO) δ 150.29, 149.45, 145.97, 145.21, 143.00, 128.56, 124.38, 124.24, 111.65, 111.36, 61.22, 50.54, 49.50, 31.15, 27.27, 27.15, 26.75, 26.27, 25.86. MS: 618 $(M -2Br)^+$

The chromatographic analysis of Ziapin2 was performed by means of a Waters HPLC system equipped with a Waters 600 Controller, a Waters 996 Photodiode Array Detector and a Jupiter 5μ C18 300A Phenomenex column. The measurement was carried out using a gradient program with 25% CH_3CN / 75% H_2O (both HiPerSolv Chromanorm grade solvents, from VWR Chemicals) initial eluent mixture for 5 min progressively modified into 100% CH_3CN over a total period of 25 min. The spectrum of the isolated compound absorbs at nearly 470 nm.

UV-VIS absorption measurements. For the UV-VIS absorption measurements, we used a Perkin Elmer Lambda 1050 spectrophotometer, equipped with deuterium (180-320 nm) and tungsten (320-3300 nm) lamps and three detectors (photomultiplier 180-860 nm, InGaAs 860-1300 nm and PbS 1300-3300 nm). For further details see Supplementary Information.

Photoluminescence measurements. The PL measurements in solution (25 μM in DMSO, water and sodium dodecyl sulfate (SDS; 100 mM) were taken with a Horiba Nanolog Fluorometer, equipped with a xenon lamp, two monochromators and two detectors (photomultiplier and InGaAs). Human Embryonic Kidney-239 cells (Hek293), used as a source of cell membranes, were obtained from ATCC. The emission of azobenzene in the membrane environment at 450 nm was elicited by using a CW diode laser (excitation energy of 10 mW mm^{-2}, matching the one of electrophysiology experiments). The emission was collected with a 50x objective (Zeiss), filtered to remove the wavelength excitation and sent to the camera (Hamamatsu, acquisition time 100 ms). The system was illuminated for a shorter time (10 s) than the PL measurements in solution, to avoid cells damaging. For further details see Supplementary Information.

Molecular dynamics (MD) simulations. All-atom Molecular Dynamics (MD) simulations of Ziapin2 in *trans* and *cis* conformations in a model membrane bilayer of 1-palmitoyl-2-oleoyl-phosphatidylcholine (POPC) made of 160 lipid molecules (80 per leaflet) and water. A starting conformation for the bilayer in water was generated using pre-equilibrated lipid structures from the CHARMM-GUI webserver (41). All simulations were run with NAMD v2.12 code (42) using the CHARMM36 force field (43) and TIP3P model for water molecules. CHARMM-compatible topology and parameters for Ziapin2 were obtained using the CHARMM General Force Field (CGenFF), and atomic charges were calculated at the B3LYP/cc-pVTZ level. The total electrostatic charge of each system was neutralized by the addition of physiological concentrations of counter ions. The time-step for integrating the equation of motion was 2 fs. Simulations were performed using periodic boundary conditions (PBC) in the NPT ensemble, i.e.

at constant pressure (1 atm) and temperature (310 K), using a Langevin piston with a constant decay of 100 ps^{-1} and an oscillation period of 200 fs and a Langevin thermostat with a damping constant of 5 ps^{-1}. Flexible unit cell was used with constant ratio in the x-y plane. Long-range electrostatic interactions were computed using the Particle Mesh Ewald method, with a fourth-order spline and 1 Å grid spacing. The PC/water system was simulated for 30 ns to equilibrate, and then the following simulations were performed: three runs of spontaneous *trans* Ziapin2 insertion in the membrane (two for 175 ns and one for 300 ns); two runs of a single Ziapin2 in the membrane, one in *trans* and one in *cis* conformation (200 ns each); two runs each with four copies of Ziapin2 in the membrane, in *trans* and *cis* conformation (200 ns each); two runs each with eight copies of Ziapin2 in the membrane, in *trans* and *cis* conformation (200 ns each); one run with sixteen copies of Ziapin2 in the membrane in *trans* conformation (200 ns). When multiple copies of Ziapin2 were considered, they were distributing symmetrically in the upper and in the lower leaflet, aligned with the respective lipid headgroups. For the *cis* systems, the initial positions were determined by aligning the pyridine branches with those of the *trans* molecules. To determine the free energy profile for moving Ziapin2 from bulk water into the PC bilayer we integrated a set of mean force values (i.e. minus the derivative of the free energy) calculated at 34 different positions of the molecule along the axis normal to the bilayer. The different values of the mean force were computed by restraining the center of mass of the pyridine nitrogen atoms of Ziapin2 at positions spaced by 1 Å along the normal with a force constant of 100 $kcal \cdot mol^{-1} \cdot Å^{-2}$. The center of mass of the bilayer was kept fixed in all mean force simulations. At each position the simulation lasted for 10-20 ns, until convergence of the mean force estimator was observed. To simulate the effect of light-induced *trans*→*cis* Ziapin2 conformational change on the membrane, we extracted a pinched bilayer conformation from the simulation with eight *trans* Ziapin2, deleted the photochromic molecules, inserted eight Ziapin2 in *cis* conformations and run a standard MD trajectory for 200 ns. For further details see Supplementary Information.

Atomic force microscopy. Atomic force microscopy data were acquired using an Oxford Instrument Cypher AFM, equipped with a liquid droplet probe holder. AFM scans were acquired in liquid in AC mode (free amplitude ~6 nm) using BL-AC40TS cantilevers (Olympus), with a nominal resonance frequency in air of 110 kHz and a nominal spring constant of 0.09 N/m.

Liposomes were prepared as previously reported (46). Bilayers were prepared starting from a 6 mg/ml large unilamellar vesicles (LUV) solution in phosphate buffer (150mM NaCl, 15 mM sodium phosphate, pH 7.4), exposed to Ziapin2 (2 mM in DMSO) for 7 min at RT, at a molar ratio lipid/Ziapin2 of around 50. In control experiments we added to the LUVs instead of the Ziapin2 solution, the same volume of pure DMSO. Samples were then diluted in phosphate buffer at a final lipid concentration of 2 mg/ml (PC bilayers) or of 1 mg/ml (ternary membranes, PC:SM:Chol 1:1:1 - mol:mol:mol), and supplemented with 1 mM $CaCl_2$ to help the vesicle fusion on the mica substrate. SLB were deposited on freshly cleaved mica discs (Ted Pella), incubating for 10 min a 100 μl droplet of the LUV/Ziapin2 (LUV/DMSO) suspension. Excess of vesicles was removed by gently washing the samples with phosphate buffer. At least three samples for every condition were analyzed. Data were imported in ImageJ for image plane fitting and line-by-line flattening, rendering and analysis.

Planar lipid bilayer experiments. Solvent-free planar lipid membranes (PLM) were formed over a 100–180 μm diameter hole sparkling drilled in a 25-μm thick Teflon septum thus separating two compartments, as previously described (47). Each chamber was filled with 2 mL buffer solution (150 mM NaCl, 15 mM sodium phosphate, pH 7.4) and stable bilayers were formed between the two chambers. Micromolar concentrations of Ziapin2 (5 μM) were sequentially added to the *cis* and to the *trans* sides of a stable preformed bilayer. Lipid compositions used were pure PC or PC:CHO:SM 57:33:10 (molar ratio). Currents were recorded with a patch-clamp amplifier (Axopatch 200B, Axon Instruments) and a PC equipped with a DigiData 1550 A/D converter (Axon Instruments) was used for data acquisition. Current traces were filtered at 2 kHz and acquired at 10 kHz by the computer using Clampex 10.5 software (Axon Instruments). All measurements were performed in the dark at room

849 temperature. Membrane capacitance was measured via continuous symmetrical triangular ramps (100
850 Hz in frequency), as summarized in Schmitt and Koepsell (48). The membrane capacitance (C_m) is
851 connected to the membrane characteristic features, e.g. area (A) and thickness (d), through the
852 following equation (1):
853 (1) $C_m(pF) = A(nm^2)\ \epsilon_r\epsilon_0\ (pF/nm) / d(nm)$
854 For a stable membrane formed by a defined lipid class or composition, we can consider A and ϵ_r being
855 constant for each experiment, therefore a measured increase in the membrane capacitance reflects a
856 linear reduction in the membrane thickness. The membrane capacitance (C_m) was obtained by
857 subtracting the capacity of the septum, which is 30 pF in our conditions.
858
859 **Electrophysiology.** Whole-cell patch-clamp recordings of Hek293 cells and low-density primary
860 hippocampal neurons (between 14 and 18 days in vitro, DIV) were performed at room temperature
861 (22-24 °C) using 3-4 MΩ borosilicate patch pipettes (Kimble, Kimax, Mexico) and under GΩ patch
862 seal. Cells with leak currents > 200 pA or series resistance (R_s) > 15 MΩ were discarded. The R_s was
863 compensated 80% (2 µs response time) and the compensation was readjusted before stimulation. The
864 shown potentials were not corrected for the measured liquid junction potential (9 mV). Voltage-clamp
865 recordings were sampled at 20 kHz and low-pass filtered at 4 kHz. Current-clamp recordings were
866 sampled at 50 kHz and low-pass filtered at 10 kHz. Patch-clamp recordings were carried out using
867 either an Axopatch 200B (Molecular Devices, San José, CA) or an EPC10 (HEKA Elektronik,
868 Reutlingen, Germany) amplifier.
869 For Hek293 cell recordings, patch electrodes (3–4 MΩ) were filled with an intracellular solution
870 containing (mM): 140 NaCl, 2 $MgCl_2$, 5 Hepes (pH 7.4). Cells were bathed during whole-cell
871 recordings in an extracellular solution containing (mM): 140 NaCl, 2 $MgCl_2$, 5 Hepes (pH 7.4) unless
872 stated in the text. For recordings in primary neurons, the standard extracellular solution contained (in
873 mM): 135 NaCl, 5.4 KCl, 1 $MgCl_2$, 1.8 $CaCl_2$, 5 Hepes, 10 glucose adjusted to pH 7.4 with NaOH. The
874 standard intracellular solutions contained (in mM): 126 K-Gluconate, 4 NaCl, 1 $MgSO_4$, 0.02 $CaCl_2$,

875 0.1 EGTA, 10 Glucose, 5 Hepes, 3 ATP-Na_2, and 0.1 GTP-Na. When indicated, recordings were
876 performed in the presence of the synaptic blockers D-AP5 (50 µM)/CNQX (10 µM) and bicuculline
877 (BIC; 30 µM) (Tocris, Bristol, UK) to block excitatory and inhibitory synaptic transmission, respectively.
878 To investigate the contribution of ionic conductances in the capacitive currents evoked by light
879 stimulation, the standard internal solution was used in combination with an extracellular solution where
880 Na^+ was replaced by choline or, alternatively, an "*external blocking solution*" containing (mM): NaCl
881 130, TEA Cl 3, $CaCl_2$ 1.8, $MgCl_2$ 1, $CdCl_2$ 5, $NiCl_2$ 1, $GdCl_3$ 1, Hepes 5, Glucose 10, Ouabain 1, in the
882 presence of 30 µM Tetrodotoxin (TTX), in combination with an "*internal blocking solution*", containing
883 (mM): CsMES 120, NaCl 4, $CaCl_2$ 0.02, EGTA 0.1, $MgSO_4$ 1, phosphocreatine 10, ATP-Na_2 3, GTP-
884 Na 0.1, Hepes 10 was used. Solution exchange was performed using gravity flow controlled by pinch
885 valves (Warner Instruments, Hamden, CT). All chemicals were purchased from Sigma Aldrich (St.
886 Louis, MO, USA), except for TTX from Tocris.
887 *Capacitance recordings.* Capacitance measurements were performed using the “sine + dc” method
888 (49,24,25) implemented as the ‘‘sine 1 dc’’ feature of the PULSE lock-in module (50). A sine wave
889 function (1-5 mV peak-to-peak) was superimposed to the holding potential of -70 mV at a frequency of
890 150-300 Hz corresponding to the C_m sampling rates. To determine changes of membrane capacitance
891 induced by light stimulation in Ziapin2-treated cells, the C_m was first averaged over 500 ms preceding
892 the light stimulus and then subtracted from the peak value induced by the stimulation.
893 *Equivalent circuit simulations.* We numerically solved the equivalent circuit as shown in Fig.S13,
894 starting from the equilibrium position according to the input parameters E = -60 mV, starting capacity
895 C_m = 30 pF, 1/*g* = 300 MΩ. The RC time constant of the circuit was 90 µs. In the simulation, we
896 changed C_m in time and calculated the predicted V_m, by keeping *g* constant, according to the
897 experimental observations.
898 *Data analysis.* Data were analyzed using pCLAMP 10 or FitMaster v2x90.1, together with Prism 6.07
899 (GraphPad) and OriginPro 9 (OriginLab) softwares
900 For further details see Supplementary Information.

Photostimulation. Illumination of neurons during electrophysiological experiments for both Ziapin2 and ChETA was provided by an LED system (Lumencor Spectra X) fibre-coupled to an upright Nikon FN1 microscope. The light source emission peaked at 470 nm to match the Ziapin2 absorption spectrum and the power density of 20 mW/mm^2, as measured at the output of the microscope objective.

***In vivo* experiments.** *Surgery.* Mice were anaesthetized with Isoflurane and placed in a stereotaxic frame, where anesthesia was maintained with an isoflurane flow. Ziapin2 (200 μM in 1 μl 10% DMSO in PBS) or vehicle was injected with a 5 μl Hamilton syringe in the primary somatosensory cortex (S1ShNc) of the left hemisphere using the following stereotaxic coordinates: 2 mm anterior to lambda, 2 mm lateral to midline, and – 723 μm ventral to brain surface. Injection was done at a rate of 100 nl/min with a nano-jector (World Precision Instruments, Fl, USA). Five minutes after, to let the molecules diffuse within brain tissue, the craniotomy was extended by 1 mm laterally and 1 mm medially to accommodate the microwire array (16 electrodes in 2 rows of 8, 33 μm diameter, 250 μm pitch, 375 μm between rows (Tucker Davis Technologies). The two central microwires were inserted at a depth of 723 μm, before being cleaned with saline and topped with silicone sealant (Kwik-cast, WPI). A hole was drilled 1 mm caudally to the injection hole and a fiber optic cannula (MFC_400/430-0.66_10mm_ZF1.25_FLT, Doric Lenses) was inserted at a depth of 1 mm and an angle of 65° from the vertical. Two surgical screws were inserted in the skull contralateral to the implants to be used as reference/ground for the microwires and support. The skull was then covered with dental cement and Diclofenac was systemically administered at a dose of 100 μl/20 g. *In vivo recordings*. For the evaluation of the acute effects of Ziapin2 loading, *in vivo* optical stimulations were performed in freely moving C57BL6 mice that had been previously injected with either DMSO (N=3) or Ziapin2 (N=3) and left to recover for 60 min before electrophysiological recordings. Light stimulation was delivered at 0.25 Hz with 40 % jitter for either 20 or 200 ms at irradiances of 4, 25, 43 or 116 mW/mm^2 with a 473

nm laser (Shanghai Dream Lasers) to the freely moving rats. Each condition was repeated 25 times. Extracellular signals in response to stimulation were amplified, digitized and sampled at 1017 Hz by commercially available hardware (System 3, Tucker-Davis Technologies) before being saved for offline analysis using custom Matlab scripts (The Mathworks). During acquisition, data were high-pass (1 Hz) and low pass (100 Hz) filtered to extract local field potentials (LFPs). The peak amplitude of the LFP waves, recorded within the correct latency range after the light onset, was normalized by the averaged noise amplitude calculated from the non-responding channels over the same epoch. For the analysis of the persistence of the Ziapin2 effects over time, implanted C57BL6 mice that had been injected with either DMSO (N=3) or Ziapin2 (N=4) at time = 0 were photostimulated and recorded as described above 1, 4 and 7 days after Ziapin2 administration. Mice that received Ziapin2 injection, but were not implanted, were euthanized at the same times after the injection and the brain processed for Ziapin2 fluorescence microscopy and immunohistochemical analysis of astro- and micro-glial reaction.

For further details about **Numerical model of the PL signal dynamics in solution, Total Internal Fluorescence Microscopy (TIRFM), Primary neuron preparations, Differentiation of human neurons from induced pluripotent stem cells, Cell Viability Assays, Fluorescence imaging of the plasma membrane, Immunofluorescence Staining and Statistical analysis** see Supplementary Information.

Figure 1

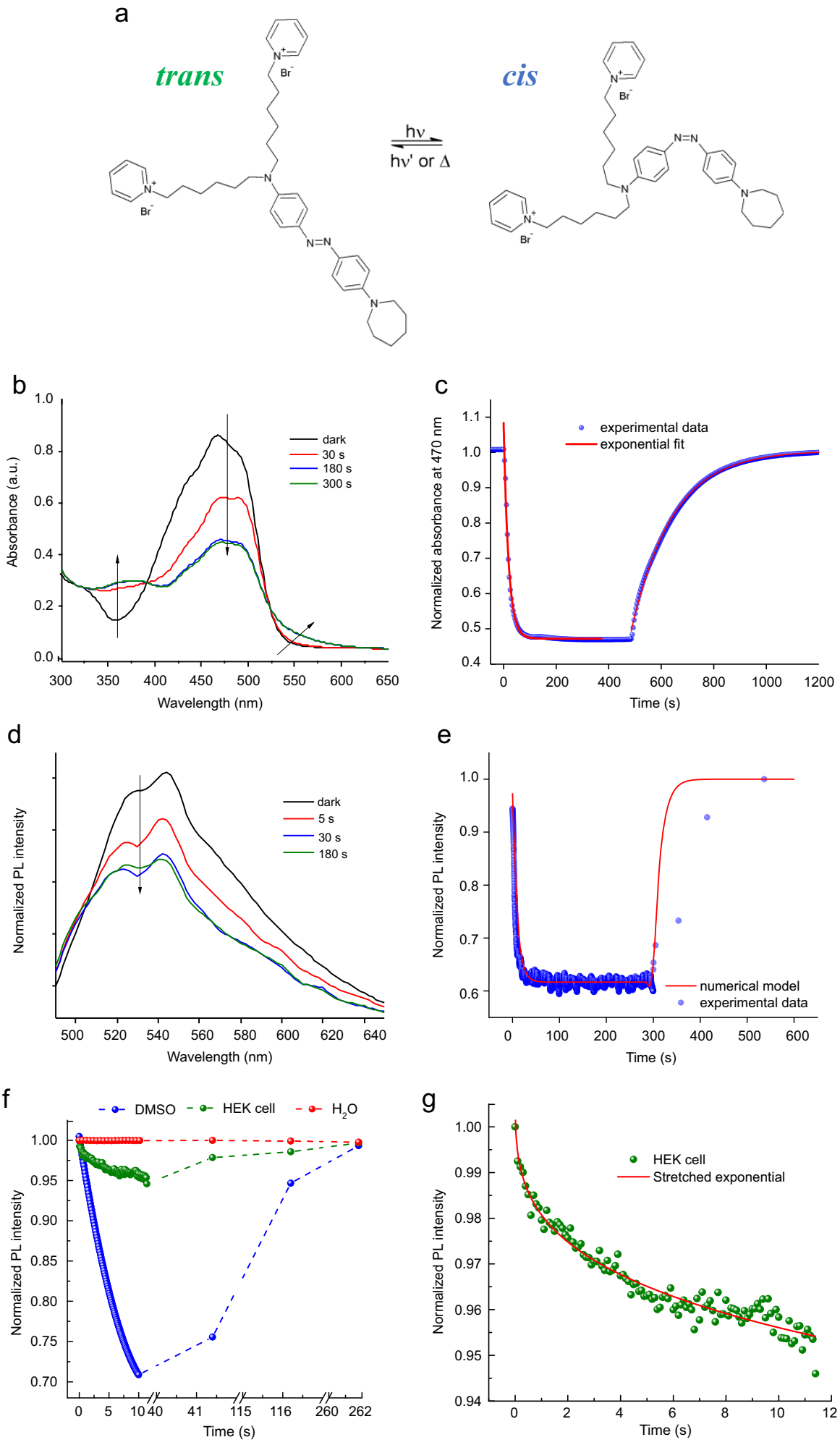
a
trans
cis
hν
hν' or Δ
Br⁻
N=N
b
Absorbance (a.u.)
Wavelength (nm)
dark
30 s
180 s
300 s
c
Normalized absorbance at 470 nm
Time (s)
experimental data
exponential fit
d
Normalized PL intensity
Wavelength (nm)
dark
5 s
30 s
180 s
e
Normalized PL intensity
Time (s)
numerical model
experimental data
f
DMSO
HEK cell
H2O
Normalized PL intensity
Time (s)
g
Normalized PL intensity
Time (s)
HEK cell
Stretched exponential

Figure 2

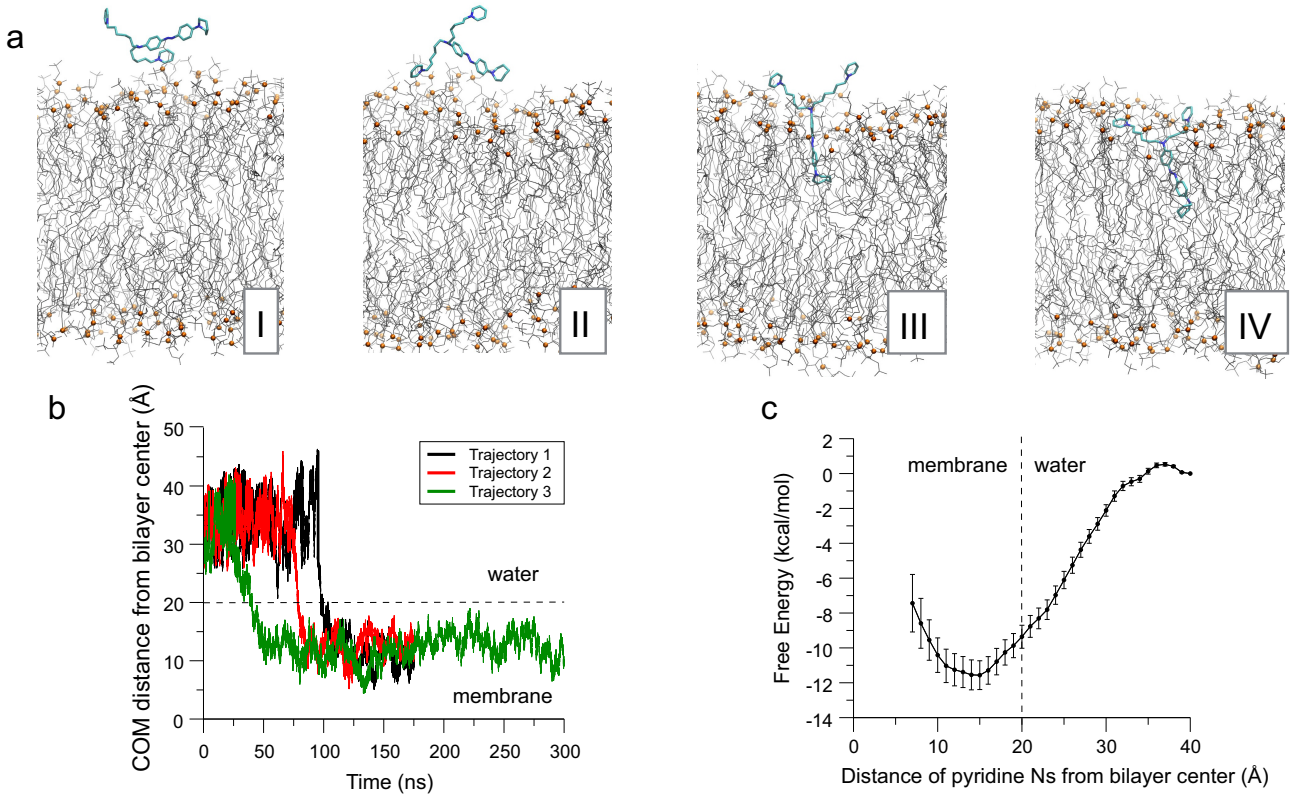
a
I
II
III
IV
b
COM distance from bilayer center (Å)
Trajectory 1
Trajectory 2
Trajectory 3
water
membrane
Time (ns)
c
membrane
water
Free Energy (kcal/mol)
Distance of pyridine Ns from bilayer center (Å)

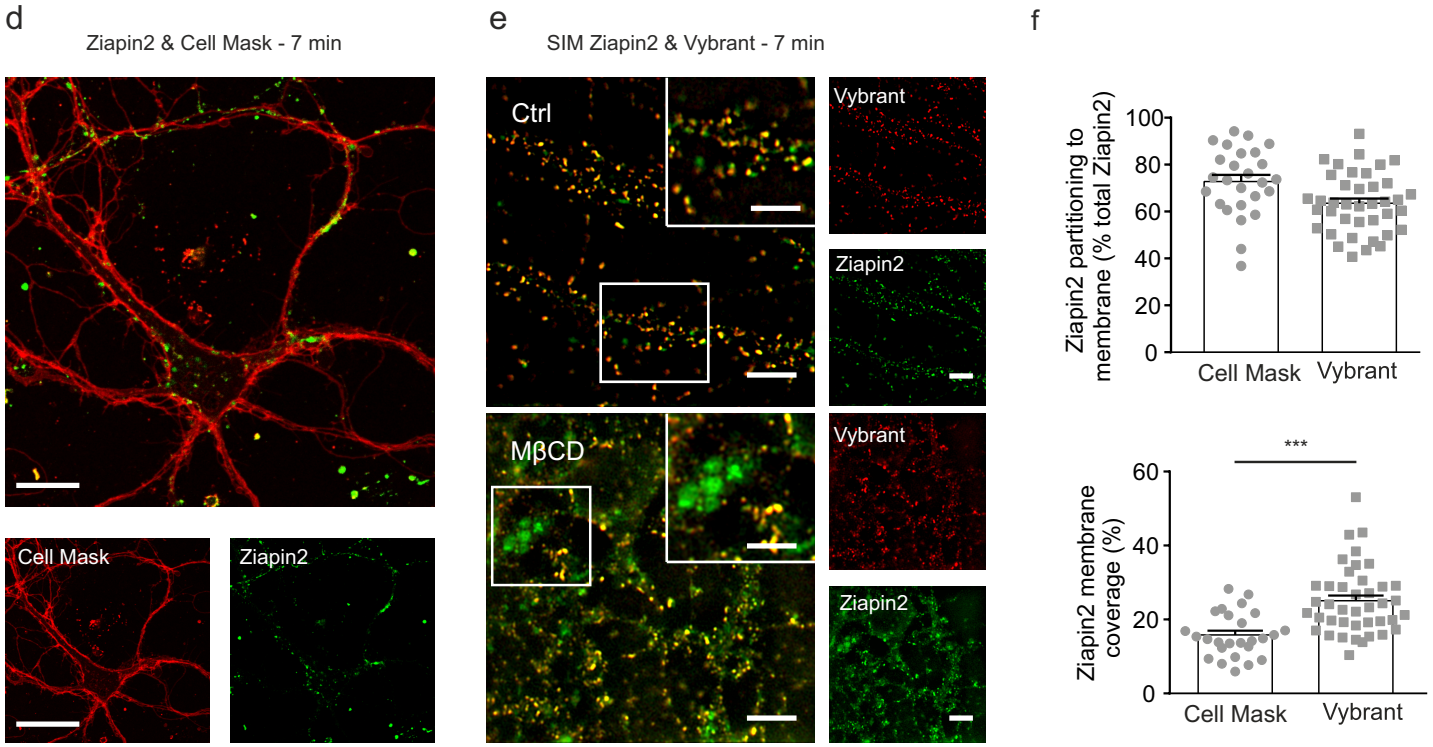
d
Ziapin2 & Cell Mask - 7 min
Cell Mask
Ziapin2
e
SIM Ziapin2 & Vybrant - 7 min
Ctrl
MβCD
Vybrant
Ziapin2
f
Ziapin2 partitioning to membrane (% total Ziapin2)
Cell Mask
Vybrant
Ziapin2 membrane coverage (%)
***

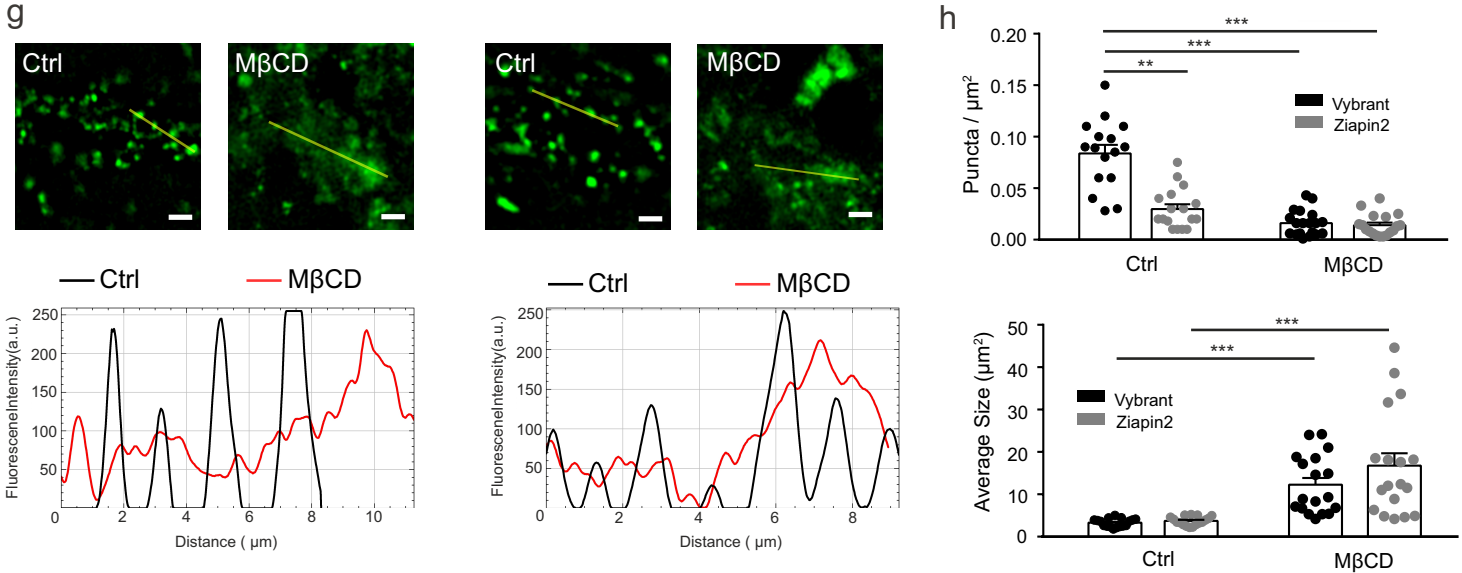
g
Ctrl
MβCD
Fluorescene Intensity (a.u.)
Distance (μm)
h
Puncta / μm²
Vybrant
Ziapin2
Average Size (μm²)
***
**

Figure 3

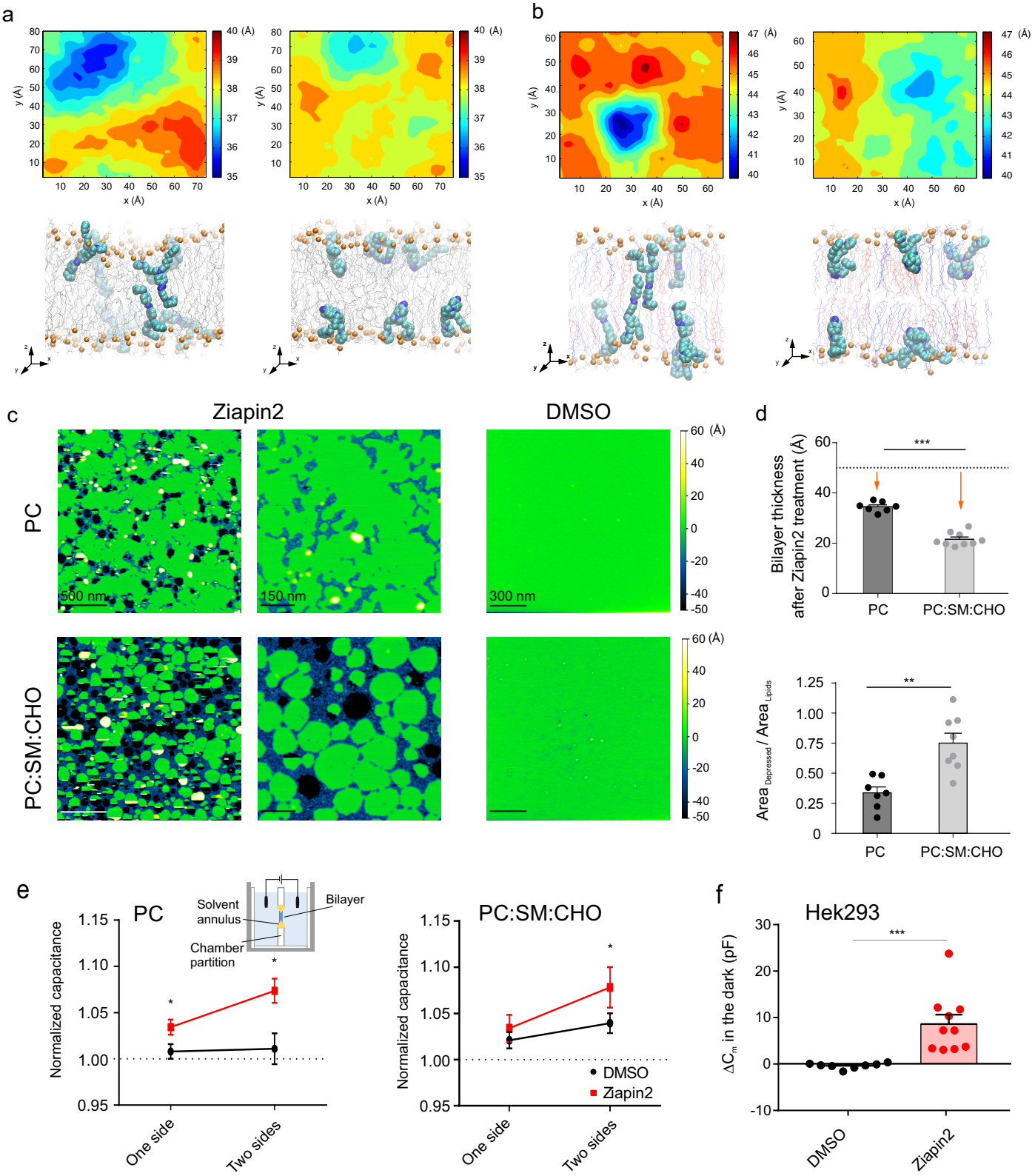
a
b
c
Ziapin2
DMSO
PC
PC:SM:CHO
500 nm
150 nm
300 nm
d
Bilayer thickness after Ziapin2 treatment (Å)
PC
PC:SM:CHO
Area Depressed / Area Lipids
e
PC
PC:SM:CHO
Solvent annulus
Bilayer
Chamber partition
Normalized capacitance
One side
Two sides
DMSO
Ziapin2
f
Hek293
ΔCm in the dark (pF)

Figure 4

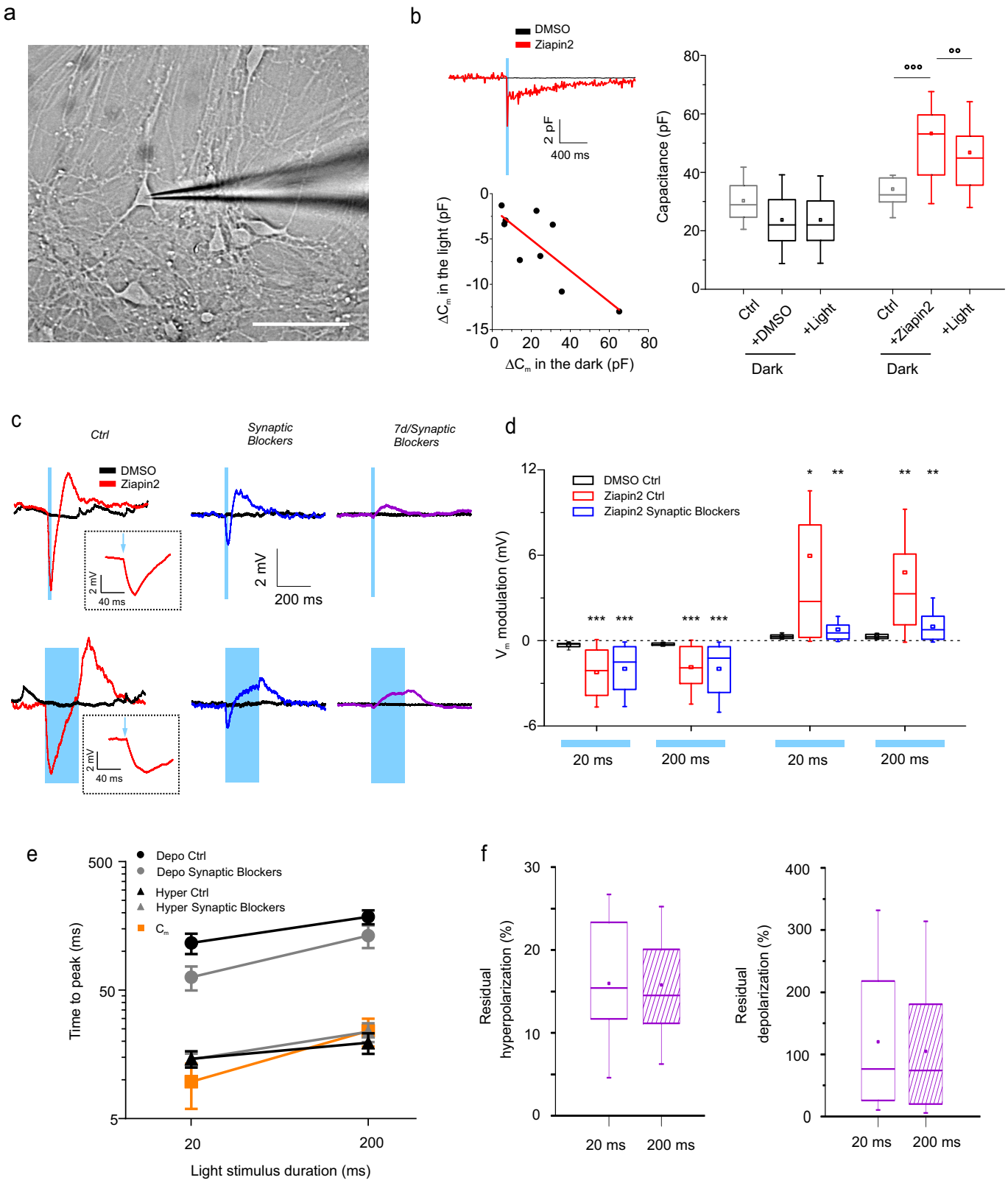
a
b
DMSO
Ziapin2
2 pF
400 ms
ΔCm in the light (pF)
ΔCm in the dark (pF)
Capacitance (pF)
Ctrl
+DMSO
+Light
Dark
+Ziapin2
c
Ctrl
Synaptic Blockers
7d/Synaptic Blockers
2 mV
40 ms
200 ms
d
DMSO Ctrl
Ziapin2 Ctrl
Ziapin2 Synaptic Blockers
Vm modulation (mV)
20 ms
200 ms
e
Depo Ctrl
Depo Synaptic Blockers
Hyper Ctrl
Hyper Synaptic Blockers
Cm
Time to peak (ms)
Light stimulus duration (ms)
f
Residual hyperpolarization (%)
Residual depolarization (%)

Figure 5

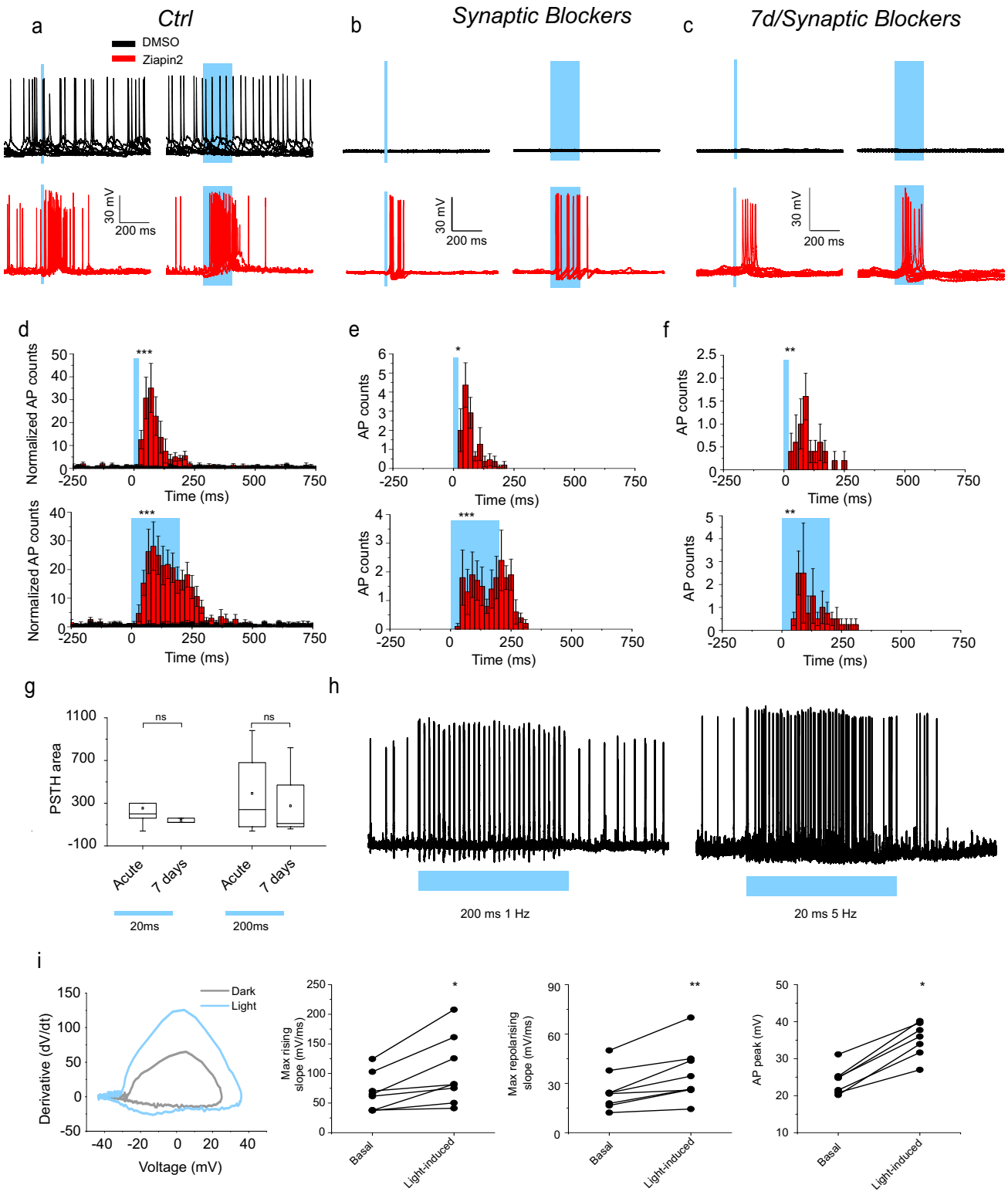
a
Ctrl
DMSO
Ziapin2
30 mV
200 ms
b
Synaptic Blockers
30 mV
200 ms
c
7d/Synaptic Blockers
30 mV
200 ms
d
Normalized AP counts
Time (ms)
e
AP counts
Time (ms)
f
AP counts
Time (ms)
g
PSTH area
ns
Acute
7 days
20ms
200ms
h
200 ms 1 Hz
20 ms 5 Hz
i
Dark
Light
Derivative (dV/dt)
Voltage (mV)
Max rising slope (mV/ms)
Max repolarising slope (mV/ms)
AP peak (mV)
Basal
Light-induced

Figure 6

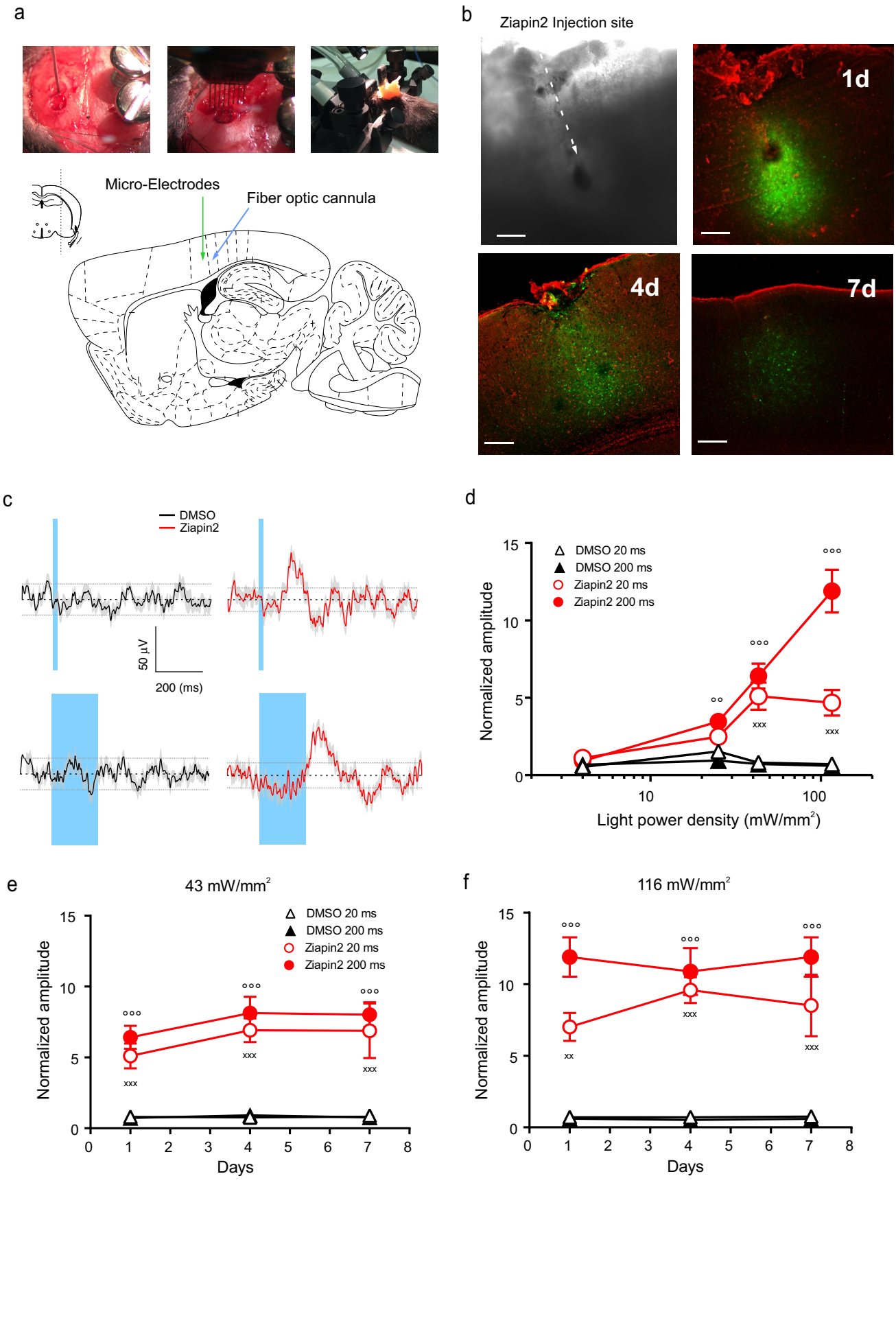
a
Micro-Electrodes
Fiber optic cannula
b
Ziapin2 Injection site
1d
4d
7d
c
DMSO
Ziapin2
50 µV
200 (ms)
d
DMSO 20 ms
DMSO 200 ms
Ziapin2 20 ms
Ziapin2 200 ms
Normalized amplitude
Light power density (mW/mm²)
e
43 mW/mm²
Normalized amplitude
Days
f
116 mW/mm²
Normalized amplitude
Days